New constraints on Chewings-aged deformation and metamorphism of ca. ≥1750 Ma crust in the Reynolds Range, central Australia

Mathew Reid

November 2012

TITLE

New constraints on Chewings-aged deformation and metamorphism of ca.$\geq$ 1750 Ma crust in the Reynolds Range, central Australia

RUNNING TITLE

Mathew D. Reid

ABSTRACT

U-Pb monazite and zircon geochronology from Proterozoic high-temperature, low-pressure granulite facies rocks within the Reynolds Range of the Arunta complex in central Australia provide constraints on the timing of magmatism, fabric development and metamorphism. Monazite age data preserves a Meso-Proterozoic age population (c.1570-1550 Ma) while zircon age analyses preserve a Paleo-Proterozoicage population (c.1775-1755 Ma). The varying response of zircon and monazite to differing conditions allows for constraints on magmatism and metamorphism. Long lived Chewings age metamorphism is constrained by monazite grains analysed from the Napperby Gneiss, metapelite and leucosomes of the Woodforde River valley. Zircon analyses defines the ca. 1765 Ma population and is from the same rock types as the monazite samples, zircon morphologies are commonly euhedral and commonly oscillatory zoned with thin to larger dark overgrowths prominent in garnet bearing leucosomes. Overgrowths commonly record younger ages than the cores with a cryptic record of c.1630-1620 Ma evident in rare grains that could support evidence for extensional tectonism in the Aileron province. Two fabrics, S3 and S4, are commonly seen in outcrop in the Napperby gneiss and Reynolds Range group and they define an intersection lineation that plunges gently to moderately to the ESE.
The main penetrative fabric within the Reynolds Range (S3; this study) is dated to be Chewings age, with this age established from monazite in cordierite, sillimanite bearing metapelite. This study shows that zircon and monazite should be used in conjunction with each other in order to establish a solid interpretation of tectonothermal events.

KEYWORDS

TABLE OF CONTENTS

1 LIST OF FIGURES AND TABLES

2 INTRODUCTION

The Arunta Region in central Australia defines the southern portion of the North Australian Craton (NAC) Fig.1. The Arunta Region is believed to have a pivotal role in understanding the assembly and/or growth of the Australian continent during the Proterozoic (Zhao & McCulloch 1995, Wade *et al.* 2006) owing to the large number (at least six) of cryptic magmatic and/or tectonic events that are recorded over a protracted period of approximately 300 Myr from ca. 1860 Ma to ca. 1550 Ma (Collins & Shaw 1995, Williams *et al.* 1996, Hand & Buick 2001, Rubatto *et al.* 2001, Betts & Giles 2006, Claoue-Long *et al.* 2008a). The large number of events recorded by rocks in the Arunta Region provides a significant challenge for unravelling the prevailing tectonic environment that created and shaped the Arunta Region. However, there is an entrenched view that the southern margin of the NAC represents a long-lived (approximately 300 Myr) active margin in many large-scale tectonic models (Giles *et al.* 2002, Scrimgeour *et al.* 2005, Betts & Giles 2006, Cawood & Korsch 2008).

In order to understand the tectonic environment of events that underpin large-scale tectonic models, fundamental data sets such as structurally constrained geochronologic and pressure-temperature data are required. However, perhaps owing to the large size of the Arunta Region (approximately 200,000 km^2; (Shaw *et al.* 1984)), there have been comparatively few such studies undertaken. This study has focussed on a region of the southeastern Reynolds Range in the central-southern Arunta Region (Fig 1). The Reynolds Range is a classic example of an obliquely exposed belt of high-temperature–low-pressure (HTLP) metamorphism (Dirks & Wilson 1990, Dirks *et al.* 1991, Vry *et al.* 1996, Hand & Buick 2001, Rubatto *et al.* 2001). A large number of studies have

been undertaken in the Reynolds Range, including the provision of a comprehensive structural framework (Dirks & Wilson 1990) and a number of geochronology studies (Collins & Williams 1995, Vry *et al.* 1996, Rubatto *et al.* 2001) that have progressively quantified the structural framework. Indeed, a lot of the understanding of the evolution of the Arunta Complex has come from studies conducted in the Reynolds and immediately adjacent Anmatjira Ranges. However, crucially, there remain significant portions and rock types of the Reynolds Range that are data-poor and/or are characterised by ages that have yet to be sufficiently explained, e.g. the c. 1780 Ma Napperby Gneiss and enigmatic ca. 1650 Ma zircon U-Pb ages (Collins & Williams 1995).

As such, there is scope to further advance our understanding of event timelines by investigating carefully selected rocks, including the Napperby Gneiss, in key parts of the Reynolds Range. Therefore, the purpose of this study is to obtain structurally constrained geochronological and metamorphic data with the aim of constraining the age of specific magmatic rocks, fabric elements and metamorphism. The data collected in this study has direct application to the larger question of the tectonic and geodynamic significance of key timelines in Proterozoic Australia. Two key outcomes of this project are first that a single event, the ca. 1590–1550 Ma Chewings Event, is chiefly responsible for the current high-grade structural and metamorphic architecture of the Reynolds Range; and second, that zircon and monazite record very different aspects of the tectonothermal history.

3 GEOLOGICAL SETTING

3.1 Regional Geology

The geology of the Arunta Region in central Australia encompasses an approximate 200,000 km^2 region of Paleoproterozoic to Palaeozoic aged, intermediate to high grade complexes of metamorphic rocks juxtaposed against Neoproterozoic to Phanerozoic sedimentary basins (Sandiford *et al.* 2001). The Arunta Region records a complex and protracted history over an approximate 1560 Myr period from ca. 1860 to 300 Ma of numerous periods of extension manifested as sedimentation that were punctuated by periods of magmatism and/or deformation and metamorphism (Collins & Shaw 1995, Hand & Buick 2001).

Figure 1: Map showing the context of the Reynolds- Anmatjira Yalyirimbi Ranges with the study area marked in green. Adapted from Scrimgeour (2005) and Raimondo 2011.
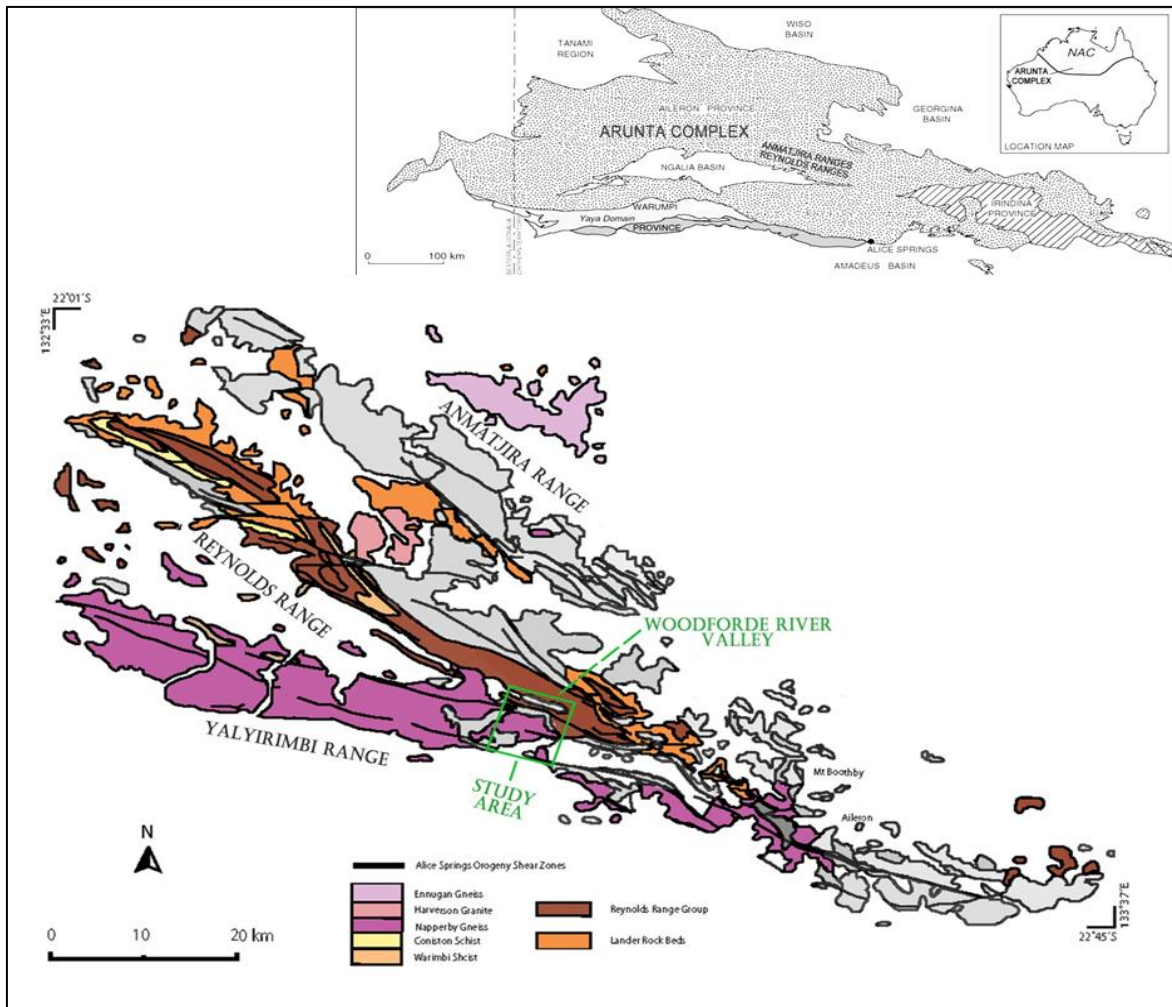
The Arunta Complex has historically been subdivided into three distinct provinces (Fig. 1) governed by differing protolith ages and histories (Scrimgeour *et al.* 2005). The provinces are the: 1) Aileron Province, which is the largest of the three provinces and contains rocks with depositional and intrusive ages between 1870–1710 Ma (Scrimgeour *et al.* 2005, Claoue-Long *et al.* 2008a); 2) Warumpi Province, which occurs on the southern margin on the Arunta Complex and has intrusive and sediment protolith ages between *ca.* 1690–1600 Ma (Scrimgeour *et al.* 2005). The Warumpi Province has been proposed to be an exotic terrane (Scrimgeour *et al.* 2005); 3) Irindina

Province, which is located in the south-eastern Arunta Region and contains sedimentary and igneous protoliths ranging from Neoproterozoic to Cambrian in age (Buick *et al.* 2001).

Event timelines that have created and shaped the Palaeo- and Meso-Proterozoic geology of the Arunta Region are detailed in Table 1 and include the Stafford Event ca. 1810-1800 Ma ;(Collins & Vernon 1991), the early Strangways Orogeny ca. 1790–1770 Ma (Collins & Shaw 1995) now known as the Yambah Event (Scrimgeour 2003), Inkamulla Igneous Event ca. 1750 Ma (Scrimgeour 2003), Strangways Event ca. 1730–1690 Ma (Möller *et al.* 2003) Liebig Orogeny ca. 1650–1630 Ma (Scrimgeour *et al.* 2005), Chewings Event ca. 1590–1560 Ma; (Shaw *et al.* 1984, Collins & Williams 1995) and the Grenvillian aged Teapot event ca. 1150–1100 Ma (Black & Shaw 1992, Morrissey *et al.* 2011). The most recent event, the Devonian to Carboniferous Alice Springs Orogeny, resulted in the exhumation of the Arunta Region from beneath the formerly contiguous Centralian Superbasin (Flottmann & Hand 1999).

.

Table 1: Summary of the main tectonothermal events that have affected the Arunta Complex, with particular emphasis on the known impact on the Reynolds-Anmatjira Ranges

Age	Event	Description
ca. 1820–1800 Ma	Stafford Event	Bi-modal magmatism and low-pressure–high-temperature metamorphism. A magmatically driven system (Collins & Vernon 1991).
ca. 1780–1770 Ma	Yambah Event	Voluminous magmatism found throughout much of the Arunta Complex. Varying degrees of metamorphism and deformation with associated magmatism previously known as the Early Strangways event (Collins & Shaw 1995). Yambah-aged metamorphism documented in the Mount Hay and Strangways range regions (Scrimgeour 2003). Contact metamorphism is evidenced around granitic precursors to the Coniston and Warimbi Schists (Fig.1) that intruded the Reynolds Range group *ca.*1785 Ma (Collins & Williams 1995, Hand & Buick 2001).
ca. 1760–1740 Ma	Inkamulla Igneous Event	Restricted mainly to the southern and eastern Arunta Complex and is deemed to be an episode of voluminous granitic and minor mafic magmatism.(Dirks *et al.* 1991), attribute this age as the emplacement of granite in the Reynolds Range, no known associated metamorphism.
ca. 1730–1690 Ma	Strangways Orogeny	Major tectonic event that resulted in *c.*1730 Ma (Möller *et al.* 2003) widespread deformation and metamorphism in the Arunta Complex (Scrimgeour 2003, Claoue-Long *et al.* 2008b). Development of Km scale folds that are defined by a folded S1 foliation (Lafrance *et al.* 1995 Intrusion of granites in the eastern Arunta and a sporadic northwest trending belt of granitic intrusions in the northern Arunta region (Collins & Shaw 1995) . Evidence of Strangways deformation is evident in the northwestern Reynolds Range (Hand & Buick 2001).
*ca.*1650–1630 Ma	Liebig Orogeny	Affected the Warumpi Province and is interpreted to be the accretion of the Warumpi Province onto the North Australian Craton. High pressure and temperature (9 kbar, 900 degC) granulite facies metamorphism in Warumpi Province. Low-angle fabrics of this age in Reynolds Range (Scrimgeour *et al.* 2005).
ca. 1590–1560	Chewings Orogeny	Variable impact across the Arunta Complex. NW to SE continuous transition from greenschist to granulite facies metamorphism in the Reynolds Range (Hand & Buick 2001). The Chewings phase of deformation (Shaw *et al.* 1984) is associated with intrusion of post tectonic pegmatite dykes in the Reynolds-Anmatjira Ranges (Collins & Williams 1995).
*ca.*1150–1130	Grenvillian-aged Teapot event	Emplacement of the Teapot Granite migmatite complex and associated pegmatites as well as migmatisation of the Gneissic basement in the southern Province(Black & Shaw 1995) . Mafic alkaline Mordor Complex emplaced in eastern Arunta Complex (Black & Shaw 1992). Significant EW-trending reworking (and metamorphism) of Warumpi and southernmost Aileron Province (Morrissey et al. 2011; Wong, 2011).
ca. 500–460 Ma	Larapinta Event	Rift-style metamorphism of Neoproterozoic to Cambrian rocks in the Irindina Province (Hand *et al.* 1999, Mawby *et al.* 1999).
*ca.*400–300 Ma	Alice Springs Orogeny	Long-lived and episodic event that resulted in exhumation of the Arunta Complex from below the Centralian Superbasin during south directed thrusting via discrete greenschist- to amphibolite-facies shear and mylonite zones (Cartwright *et al.* 1999, Flottmann & Hand 1999). Shear zones reflected in the metapelites and granites in the southeastern Reynolds range are as a result of the Alice springs orogeny (Collins & Shaw 1995, Cartwright *et al.* 1999).

3.2 Geology of the Reynolds Range

The Reynolds-Anmatjira-Yalyirimbi Ranges (Fig 1) occur in the Aileron Province and trend in a NW-SE direction for a distance of approximately 130 km. A comprehensive summary of the geology of the Reynolds Range is provided by Hand & Buick (2001); however, the salient points are covered here. Four 'packages' of rock have been recognised in the Reynolds-Anmatjira-Yalyirimbi Ranges on the basis of unconformable and intrusive relationships (Dirks & Wilson, 1990). The oldest rock package in the area and in the Arunta Region is the Lander Rock Beds, a sequence of sandstone and siltstones deposited at ca. 1840–1806 Ma (Vry *et al.* 1996, Hand & Buick 2001) based on U-Pb ages obtained by Vry *et al*. (1996). This was intruded by a series of granitic rocks (second 'package') at ca. 1815 ± 10 Ma (Collins & Vernon 1991); Table 1.

The third 'package' is the Reynolds Range Group of sediments which unconformably overlies the first two packages and is estimated to have been deposited in the interval ca. 1812–1785 Ma (Collins & Williams 1995, Hand & Buick 2001). The Reynolds Range Group comprises basal quartzite overlain by interlayered pelite, quartzite and calc-silicate (Dirks & Wilson 1990). The youngest 'package' is another series of granitic intrusions that include the Napperby Gneiss and the Boothby Orthogneiss. The age of this aerially extensive magmatic rock system has been constrained from only a small number of localities, at ca. 1780 Ma ((Collins & Williams 1995); Table 1).

The Napperby Gneiss is reported to contain a complex and poorly understood geochronological record. Ages corresponding to the Yambah/Inkamulla, Strangways and Liebig event timelines have been reported from the Napperby Gneiss (Dirks & Hand 1991, Collins & Williams 1995).

However, no systematic study has been performed on the Napperby Gneiss in order to unravel the significance of these timelines. In particular, ages of ca. 1650 Ma (Collins & Williams 1995) were obtained from soccer-ball–shaped zircons, interpreted as metamorphic, in Napperby Gneiss from the Woodforde River valley. The local and regional significance of these zircons and their age has yet to be fully understood. The ca. 1650 Ma age is intriguing as the outcrop is characterised by a sub-horizontal fabric (this study) and elsewhere in the Arunta Complex this timeline has been interpreted as subduction-related accretion of the Warumpi Province to the Aileron Province (Scrimgeour *et al.* 2005).

The Reynolds Range records a continuous transition in metamorphic grade from greenschist facies in the NW to granulite facies in the SE (Hand & Buick 2001, Rubatto *et al.* 2001). The age of this metamorphic field gradient is constrained to the ca. 1590–1560 Ma Chewings Orogeny (Vry *et al.* 1996, Williams *et al.* 1996, Hand & Buick 2001, Rubatto *et al.* 2001, Claoue-Long *et al.* 2008b).

The structural framework proposed by Dirks & Wilson (1990) is sufficiently complex that for the purposes of this study, a revised nomenclature is used. The nomenclature used herein is D_1 produces S_1, F_1, L_1; D_2 produces S_2, F_2, L_2 etc. D_1/S_1 is only preserved

in the low-grade rocks of the NW Reynolds Range and the high-grade rocks at Mt Stafford in the extreme NW of the Anmatjira Range (Dirks & Wilson 1990). This fabric is present in the Lander Rock Beds but not the Reynolds Range Group (Dirks & Wilson 1990). S_2 is only locally preserved as metamorphic minerals aligned around the hinges of F_3 folds but occurs in all four lithological packages.

The regionally dominant fabric in the Reynolds Range is here termed S_3 (referred to as SII_2 of Dirks & Wilson, 1990), which in the high-grade (SE) parts of the Reynolds Range is a composite S_0-S_2-S_3 fabric trending NW. F_3 folds trend NW-SE and are commonly isoclinal (Dirks & Wilson 1990). S_3 and F_3 can be followed continuously across the granulite to greenschist transition (Dirks & Wilson 1990), implying this event predates the metamorphic overprint. Migmatisation occurred during D_3 and produced leucosomes that are oriented parallel to S_3 and F_3axial traces. D_4 resulted in the production of conjugate sets of crenulation bands that geometrically resemble conjugate kink bands (DII_3 of Dirks & Wilson, 1990).

The scale of the conjugate kink bands ranges from kilometre-scale to millimetre-scale. The axial traces of the conjugate kink bands are oriented ENE and NW (Dirks & Wilson 1990). D_4 did not produce a penetrative fabric, but melting or melt remobilisation during D_4 resulted in leucosomes oriented parallel to F_4 axial traces (Hand & Dirks 1992). A period of retrogression is interpreted to have occurred between D_3 and D_4 (Dirks & Wilson 1990). D_5 is characterised by mylonitic shear zones (sometimes kyanite and staurolite-bearing) that are typically reactivated at lower metamorphic grade (micaceous only) during D_6 (DII_4 and $DIII$, respectively, of Dirks & Wilson

1990;(Dirks *et al.* 1991, Williams *et al.* 1996, Cartwright *et al.* 1999, Hand & Buick 2001) . Note that because the summary of fabric elements provided here was created on a largely relative age basis (Dirks & Wilson 1990) , unrelated co-linear or co-planar events may be grouped under the same 'D' group, resulting in the potential masking of some events.

3.3 Study Area

This study is focussed in part on the Woodforde River valley to specifically interrogate the same Napperby Gneiss outcrops that Collins and Williams (1995) obtained the complex array of ages from. The other region of focus for this study is the Yalyirimbi Range immediately south of Mt Airy (Fig.1).Here, the Napperby Gneiss and Reynolds Range Group dominate outcrop, and there exists no geochronological constraint on the timing of magmatism or metamorphism. Rocks in the Woodforde River valley and Yalyirimbi Range are metamorphosed to granulite-facies grade.

4 FIELD OBSERVATIONS

4.1 Woodforde River valley region

In the Woodforde River valley the Reynolds Range Group is intruded by granitic rocks, mapped as the Napperby Gneiss (Stewart 1981) . The Napperby Gneiss is a medium-grained quartzo-feldspathic unit that has a composite S_2-S_3 foliation defined by biotite. The S_3 foliation is generally a northwest-trending, layer-parallel fabric that dips shallowly (15-50 degrees) to the northeast.

Two fabrics, S_3 and S_4, are commonly observed in outcrop of Napperby Gneiss and Reynolds Range Group rock and define an intersection lineation (L_{3-4}) that plunges approximately shallowly to moderately (10 to 50) to the ESE. The two fabrics occur at a low angle to each other. The Napperby Gneiss has a high abundance of leucosomes that occur parallel to (D_3/S_3) the S_3 gneissic foliation as well as cross-cut it (D_4; Hand & Dirks, 1992). Four types/morphologies of leucosomes are present: 1) leucosomes that contain abundant 2–15 cm sized garnet poikiloblasts. These leucosomes occur parallel to S_3 as well as S_4; Fig.2a, 2) leucosomes that present large K-feldspar depletion halos surrounding the garnet and run parallel to the S_3 foliation Fig.2b;and 3) leucosomes that are finer-grained than types 1 and 2 and are isoclinally folded. These leucosomes are ascribed to the D2/S2 fabric (Fig.2c). In addition, garnet-absent granitic melt bodies have accumulated at the structural top of the Napperby Gneiss, where melt was unable to penetrate through the overlying calc-silicate (Fig.2d; Hand and Dirks, 1992). Rarely, veins of this granitic melt have cross-cut S_3 layering in the calc-silicate.
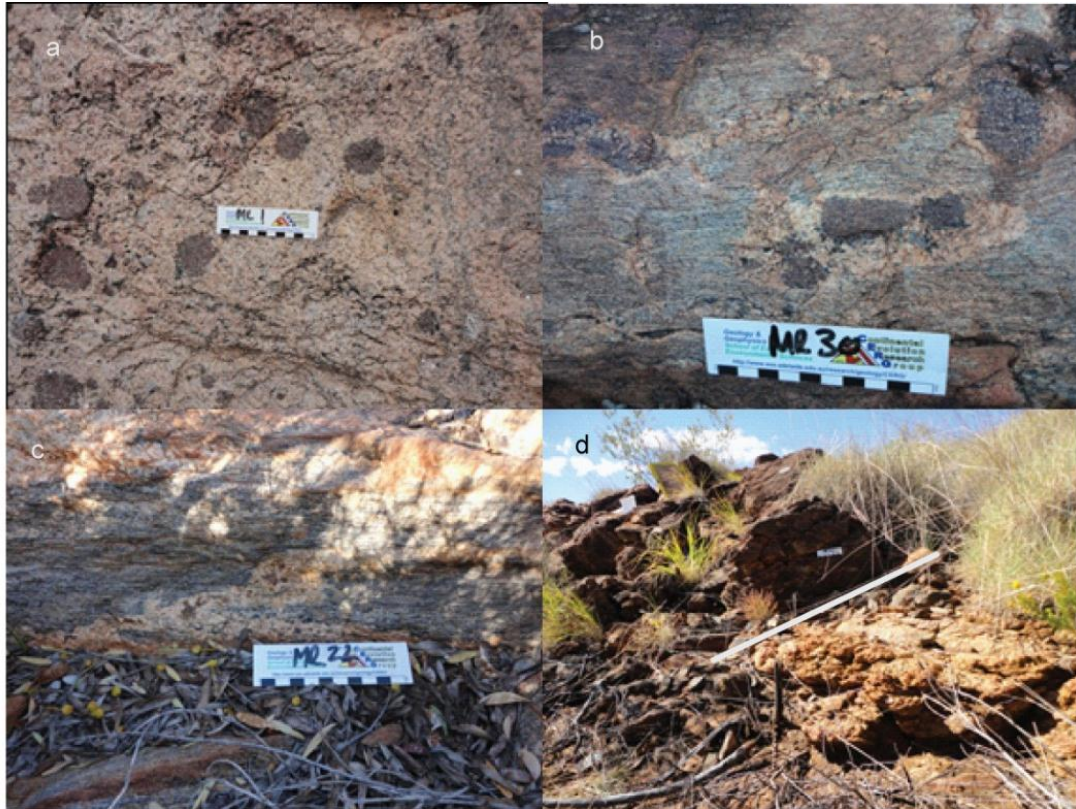
Figure 2:Photographs of the four types of leucosomes a) occur parallel to S_3 and S_4 with large 2-15cm garnet poikiloblasts; b) leucosomes that present k-feldspar rich depletion halos surrounding garnet and run parallel to foliation; c) Finer grained that a and b that are isoclinally folded and pertain to D_2/S_2 fabric; d) granitic melt that is garnet absent and has accumulated structurally on top of the Napperby gneiss and has been unable to penetrate through the overlying calc-silicate.

Calc-silicate of the Reynolds Range Group is fine-grained, epidote rich and contains andradite garnet. Spectacular deformational features are recorded by the calc-silicate. These include: 1) isoclinal F_3 folds of a composite compositional and early tectonic layering (i.e. $S_0 \| S_2$) Fig.3a; 2) Domino boudin micro-kinematic indicators in the S_3 fabric indicate a top to the North shear sense (Fig.3b) and evidence of extension (Fig.3c), whereas small scale fold vergence in the S_4 indicates a top to the south shear sense (Fig.3d); and 3) and lineation are preserved. The compositional layering of the calc-silicate is folded, and a shear fabric is developed which is defined by elongate minerals on the surface, these minerals define a new axial surface of the folds that align with the lineations plunging gently to the east.
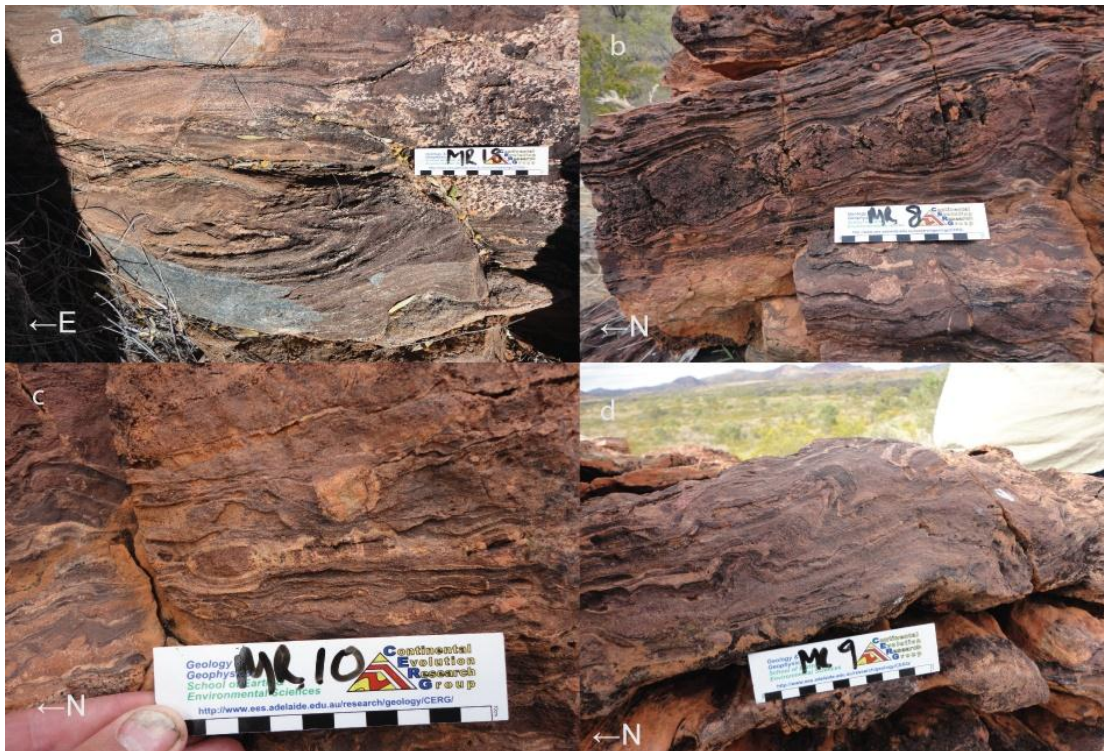
Figure 3: Calc-silicate rock that preserves spectacular structures; a) isoclinal folding of a composite compositional and early tectonic layering; b) Domino boudins indicating a top to the north shear sense; c) Interboudin dilation in the N—S orientation give micro evidence of extension; d) South vergent folds that give top to the south shear sense.

The metapelite of the Reynolds Range Group is a cordierite–sillimanite–biotite—K-feldspar quartz ± cordierite gneiss, with occasional garnet bearing layers and occurs stratigraphically between the underlying calc-silicate and overlying Mt Thomas Quartzite. Graded bedding, S_0, is rarely present in outcrop (Fig.4a) and indicates younging direction to the northeast. The metapelite preserves a bedding-parallel foliation composite S_2-S_3 defined by biotite and sillimanite (Fig.4b). Layer-parallel D_3/S_3 leucosomes that have biotite-rich selvedges/melanosomes are common (Fig.4c).
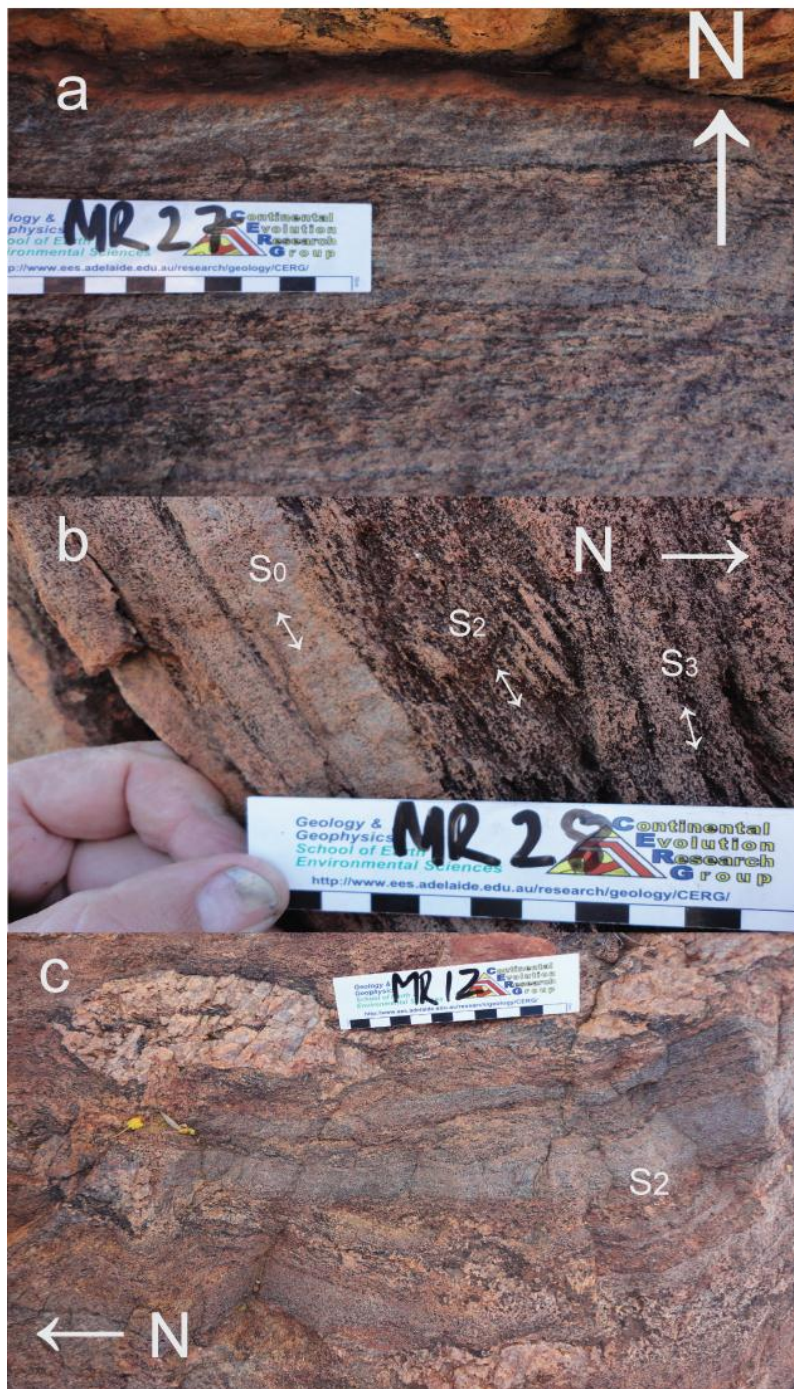
Figure 4 : Photographs of the Reynolds Range metapelite a) Rare S_0 graded bedding, fining upward seqeunce indicate younging to the north; b) the preservation of three fabrics, S_2 layer S_0 parallel fabric with a steeper S_3; c) Layer parallel D_3 leucosomes that have biotite rich melanosomes.

Rock samples for geochronological and metamorphic analysis were collected from the

Napperby Gneiss and Reynolds Range Group from a number of structural domains (see

Figs5aand 5b). In particular, rocks collected from the Woodforde River valley were collected for the specific aim of attempting to unravel the complex and not fully understood geochronology obtained by Collins et al. (1990/1). Details of the samples used in this study are provided in Table 2.

Sample location map and Schematic cross section
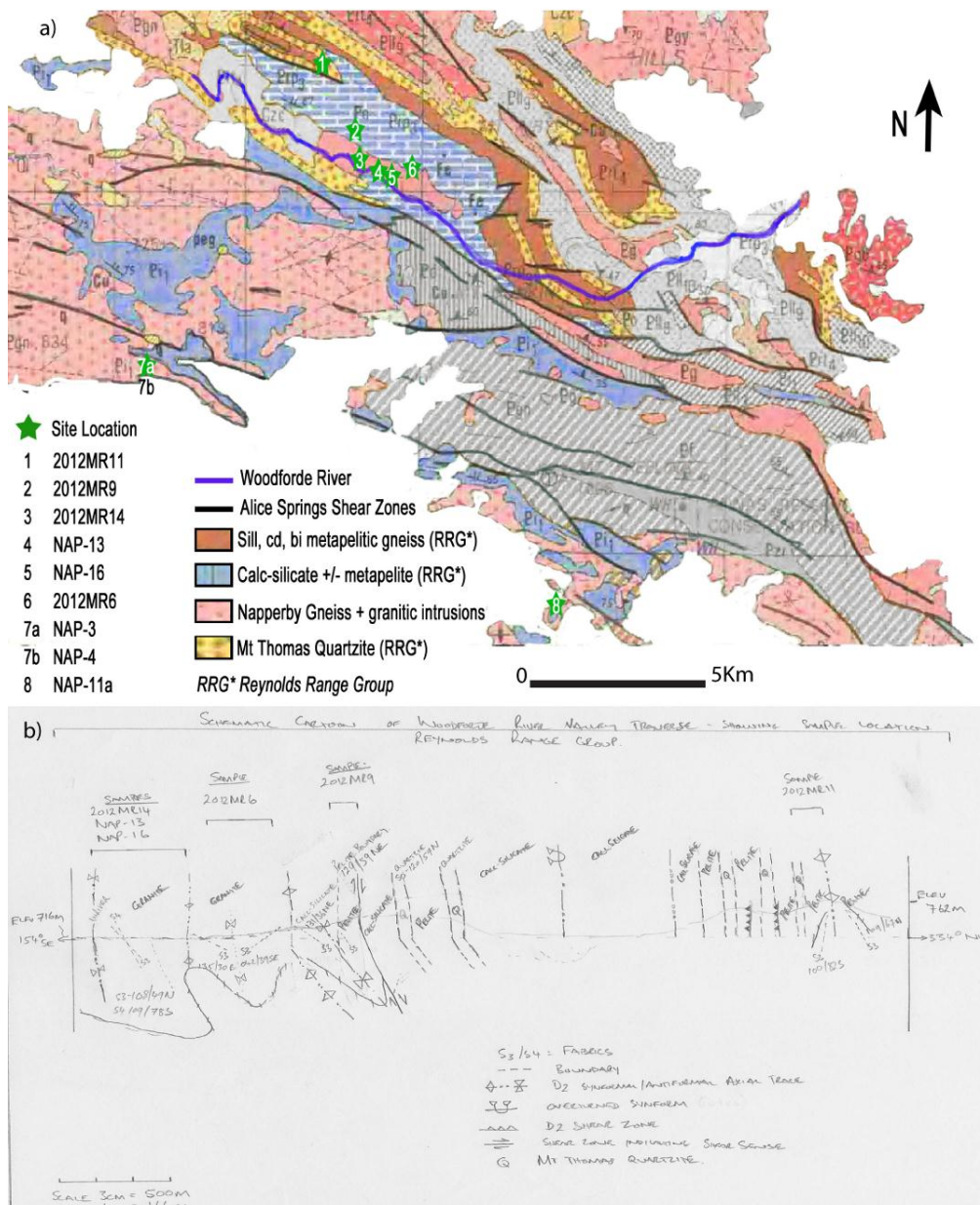
Figure 5: Sample location map within the Reynolds Yalyirimbi Range a) map of relevant units and sample locations b) rough schematic cross section displaying rough structural interpretation and areas of sample collection.

Table 2: Summary of samples analysed for U-Pb zircon and/or monazite geochronology (all samples) and metamorphic pressure-temperature (denoted by ^) work. The GPS coordinates are the UTM grid system zone 53K with the WGS84 datum. The structural domain/setting of each sample is also provided.

Sample	Easting (m)	Southing (m)	Description	Fabric orientation	Structural fabric domain
NAP-3	291163	7505462	Mylonite in Napperby Gneiss	111/84N	D_5/S_5
NAP-4	291187	7505425	Napperby Gneiss	094/83S	D_3/S_3
NAP-11a	304734	7498708	Sillimanite–cordierite–biotite–K-feldspar metapelitic gneiss	Not recorded	D_3/S_3
NAP-13	298804	7511258	Leucosome with retrogressed garnet. Garnet is retrogressed to brown and green biotite and accessory euhedral muscovite. Hand & Dirks (1992) locality.	145/80NE	D_4/S_4
NAP-16	299066	7511254	Garnet-bearing leucosome	Not recorded	D_4/S_4
2012MR6	299824	7511466	Garnet-absent leucocratic melt	Not recorded	D_4
2012MR9^	297926	7512494	Sillimanite–cordierite–biotite–K-feldspar metapelitic gneiss	129/59NE	S_3 in limb of F_4 fold
2012MR11	296866	7514502	Sillimanite–cordierite–biotite–K-feldspar metapelitic gneiss within F3 hinge	046/38SE	S_2 in F_3 fold
2012MR14	298051	7511696	Granitic gneiss with well-developed S3 and S4 fabric	116/39N S3 108/79N S4	S3 and S4 at low angle to each other in sample

5 METHODS

5.1 Whole rock composition and pressure-temperature pseudosection

Sample 2012MR9 was crushed in a jaw crusher and milled in a tungsten carbide mill. A 1 g sub-sample of fused rock powder to 4g of flux was used to prepare a fused disc for XRF major element analysis. All samples to be analysed for U-Pb zircon and/or monazite geochronology were first crushed in a jaw crusher and milled in a tungsten carbide mill.

Forward modelled phase equilibria calculations were employed to determine the physical pressure-temperature (P–T) conditions of metamorphism for the S_3 (and possibly S_4) fabric in the Woodforde River valley region. A P–T pseudosection (Fig.12) was calculated for metapelitic sample 2012MR9 using the XRF whole rock chemical composition (in mole% element) and the program Theriak-Domino (de Capitani & Petrakakis 2010).The calculation procedure is based on the minimisation of Gibbs Energy for a rock composition in a set chemical system at specified pressure and temperature nodes. The internally consistent dataset of Holland and Powell (1998; dataset tcds55 November 2003 update) was used for calculations in the geologically realistic chemical system NCKFMASHTO (Na_2O–CaO–K_2O–FeO–MgO–Al_2O_3–SiO_2–H_2O–TiO_2–Fe_2O_3).The modelling for this system uses the a–x relationships of White *et al*. (2007) for silicate melt, garnet and biotite; Coggan and Holland (2002) for muscovite; White *et al.* (2002) for orthopyroxene, spinel and magnetite; (White *et al.* 2000) for ilmenite and hematite; (Holland & Powell 1998) for cordierite; (Holland & Powell 2003) for ternary plagioclase and ternary K-feldspar.

5.2 U-Pb LA-ICP-MS Geochronology

U-Pb geochronology was conducted on zircon and monazite grains that were separated from crushed rock. Zircon and monazite were extracted from whole rock samples of approximately 1–2 kg using a crusher, tungsten carbide mill and conventional sieving (to recover grains between 79µm and 400µm) followed by panning, Frantz Isodynamic magnetic and heavy liquid separation techniques. Individual zircon and monazite grains were then hand-picked (separately), mounted in separate 2.5 cm diameter circular epoxy grain mounts and hand polished until the centre of the zircon or monazite grains was revealed. U-Pb isotopic analysis was conducted using a New Wave 213 nm Nd-YAG laser coupled to an Agilent7500cs ICP–MS at the University of Adelaide.

5.2.1 ZIRCON ANALYSIS

Zircon geochronology was used to constrain igneous and metamorphic events and to constrain the maximum depositional age of metasediments. Prior to LA–ICP–MS analysis, all zircon grains were imaged using a backscattered electron (BSE) detector and cathodoluminescence (CL) detector on a Phillips XL20 Scanning Electron Microscope (SEM) in order to identify and classify their internal structural. Convoluted, metamict zones within zircon grains were avoided during data collection.

Laser ablation was performed in a helium atmosphere, with a beam diameter of approximately 30 µm at the sample surface, a repetition rate of 5 Hz and laser intensity of 9–10 J.cm^{-2}. Each analysis consisted of a total acquisition time of 120 s, comprising of 40 s background measurement, 10 s of laser firing with the shutter closed to allow for beam stabilisation and 70 s of sample ablation.

Isotope masses were measured for 10 ms, 15 ms, 30 ms, 10 ms, and 15 ms for ^{204}Pb, ^{206}Pb, ^{207}Pb, ^{208}Pb, and ^{238}U respectively. Raw LA–ICP–MS data was processed using 'GLITTER', a data reduction program developed at Macquarie University, Sydney (Griffin *et al.* 2008). U-Pb fractionation was corrected for using the external zircon standard GJ (TIMS normalisation data: ^{207}Pb/^{206}Pb age= 607.7 ± 4.3 Ma; ^{206}Pb/^{238}U age= 600.7 ± 1.1 Ma; ^{207}Pb/^{235}U age= 602.0 ± 1.0 Ma (Jackson *et al.* 2004)).The accuracy of data correction was monitored by repeated analysis of the internal zircon standard Plešovice (ID-TIMS normalisation data: ^{207}Pb/^{206}Pb age= 337.13 ± 0.37 Ma (Slama *et al.* 2007)).Common lead was not corrected for during data reduction; however, analyses were discarded if common lead levels, indicated by proxy with the ^{204}Pbisotope, rose to levels high enough to compromise the integrity of the output age. Throughout the study, the weighted averages obtained for GJ are ^{207}Pb/^{206}Pb= 609±3.8 Ma (*n*=250, MSWD=0.52), ^{206}Pb/^{238}U= 597 ± 4 Ma (*n*=250, MSWD=14) and ^{207}Pb/^{235}U= 601 ±2.9 Ma (*n*=250, MSWD=10.3) and Plešovice are ^{207}Pb/^{206}Pb= 335 ± 5.6 Ma (*n*=119, MSWD=0..92), ^{206}Pb/^{238}U= 336 ± 1.8 Ma (*n*=119, MSWD=5.5) and ^{207}Pb/^{235}U= 336 ± 1.6 Ma (*n*=119, MSWD=4.3).

5.2.2 MONAZITE ANALYSIS

Monazite geochronology was used largely to constrain metamorphic events. Prior to analysis, all monazite grains were imaged using aback scattered electron (BSE) detector on a Phillips XL20 Scanning Electron Microscope (SEM) in order to identify internal compositional variability and to select homogeneous areas for age determination. U-Pb isotopic analyses of monazite were obtained using a similar methodology to zircon geochronology.

Ablation was performed in a helium atmosphere, with a beam diameter of approximately 15 μm at the sample surface, a repetition rate of 5 Hz and laser intensity of 9–10J.cm^{-2}. Each analytical run had a total acquisition time of 100 s, comprising 40 s of background measurement, 10 s of laser firing with the shutter closed to allow for beam stabilisation and 50 s of sample ablation. Isotopic masses were measured for 10 ms, 15 ms, 30 ms and 15 ms for ^{204}Pb, ^{206}Pb, ^{207}Pb and ^{238}U respectively. The comprehensive methodology followed for monazite isotopic analysis is outlined in Payne et al. (2008).

Raw LA–ICP–MS data was processed using the software program 'GLITTER' (as per form zircon). U-Pb fractionation was corrected for using the internal monazite standard MAdel (TIMS normalisation data: ^{207}Pb/^{206}Pb age= 491.0 ± 2.7 Ma; ^{206}Pb/^{238}U age= 518.37 ± 0.99Ma; ^{207}Pb/^{235}U age= 513.13 ± 0.19 Ma: (Payne et al. 2008)). The accuracy of data correction was monitored by repeated analysis of the in-house monazite standard 94-222/Bruna NW (ca. 450 Ma) (Payne et al. 2008). Throughout the study, the weighted averages obtained for MAdel are ^{207}Pb/^{206}Pb= 489 ±5.3 Ma (n=91, MSWD=0.76), ^{206}Pb/^{238}U= 515±2.8 Ma (n=91, MSWD=3.5) and ^{207}Pb/^{235}U= 510±2.5 Ma (n=91, MSWD=0.3.8), 222 are ^{207}Pb/^{206}Pb= 449±9.5 Ma (n=42, MSWD=1.2), ^{206}Pb/^{238}U= 453±6.2 Ma (n=42, MSWD=10) and ^{207}Pb/^{235}U= 452±5.6 Ma (n=42, MSWD=9.6).

Signals were examined carefully for portions of signal related to zones of Pb loss or gain and the best portion of each ablation signal was selected for age and error determination. Common lead was not corrected for as outlined above for zircon.

Reduced zircon and monazite data were then exported into Microsoft Excel™ (2007) where subsequent conventional concordia and weighted average plots were generated using Isoplot v4.11 (Ludwig, 2003). Ages quoted throughout the study are ^{207}Pb/^{206}Pb ages because the rocks and events are older than ca. 1100 Ma. Concordance was calculated using the ratio of (^{206}Pb/^{238}U age) / (^{207}Pb/^{206}Pb age).

6 RESULTS

6.1 Geochronology

A total of nine samples were selected for U-Pb zircon and monazite LA–ICP–MS

geochronology (Table 2). Zircon and monazite analysis was conducted on five samples

(NAP-4, NAP-11a, NAP-13, 2012MR9, 2012MR14), zircon-only analysis was

conducted on two samples (NAP-3, NAP-16) and monazite-only analysis was

conducted on two samples (2012MR6, 2012MR11). Results of zircon and monazite

geochronology are summarised in Table 3.Full U-Pb data tables for zircon and monazite

are provided in appendices A and B.

6.1.1 U-PB ZIRCON LA–ICP–MS GEOCHRONOLOGY

6.1.1.a   Sample NAP-3: Mylonite in Napperby Gneiss

Grain size was typically 50–200 μm with a typical aspect ratio of 1:3 (Fig 6f). CL

imaging showed that the majority of grains exhibited lighter, homogenous cores

bounded by dark overgrowths that were typically 2–5 μm wide. Conversely, some

grains showed darker cores while others had convoluted zoning. Oscillatory zoning was

not well defined in the majority of the grains. Twenty-nine analyses were obtained from

29 individual grains, and 6 analyses were rejected on the basis of poor spot placement

compromising those analyses. A single age population occurs and has a weighted

average $^{207}Pb/^{206}Pb$ isotopic age of 1765 ± 9 Ma (n=23, MSWD=0.26) with

concordancy of analyses within 95–105% (Fig6a). A plot of Th/U ratio vs age for NAP-

3 is shown in Fig.8a. The zircon analyses are characterised by a large cluster of Th/U

values between about 0.13 and 0.3. There are no analyses with Th/U <0.1.

6.1.1.b   Sample NAP-4: Napperby Gneiss with S3 fabric

Zircon grain size typically varied between 100–300 µm with an aspect ratio of 1:2 (fig 6g). CL imaging showed that the majority of zircon grains have cores that are typically weakly luminescent and have weak oscillatory zoning. Overgrowths are dark and measuring 2–10 µm in width. Conversely, a number of grains exhibited dark cores. Forty-four analyses were obtained from 40 grains; 16 analyses were eliminated for being <95% or >105% concordant and a further two analyses were eliminated on the basis of poor beam placement. A single (but slightly 'diffuse') age population occurs and has a weighted average $^{207}Pb/^{206}Pb$ isotopic age of 1773± 11 Ma (n=24, MSWD=1.11), with concordancy of analyses within 95–105% (Fig 6b). A plot of Th/U ratio vs age for NAP-4 is shown in Fig. 8b. The zircon analyses are characterised by a large range in Th/U values, with many clustering between about 0.1 and 0.35. A single analysis has a Th/U ratio <0.1.

6.1.1.c   Sample NAP-13: Leucosome with retrogressed garnet

Zircon morphology is variable, ranging from subhedral to equant and euhedral with a majority of grains having rounded morphologies. Under transmitted light colour varies from pale pink to dark brown crystals. Zircon grains vary from 50–180 µm with an aspect ratio of 1:2 (fig6h). CL imaging showed that the majority of grains display a weakly luminescent and zoned core surrounded by a darker overgrowth that ranges in width from 10–15 µm. Seventy analyses were conducted on 66 grains with 45 being eliminated for being <95% or >105% concordant. Isoplot™$^{207}Pb/^{206}Pb$ unmix isotopic ages of 1766± 9 Ma (n=19, 76%), and 1634 ± 17 Ma (n=6, 24%) Fig.6c.A plot of Th/U ratio vs age for NAP-13 is shown in Fig. 8c. The zircon analyses are characterised by a

large range in Th/U values, from 0.012 to 0.746, with most analyses clustering between about 0.08 and 0.25. A trend towards lower Th/U ratios with decreasing age is apparent.

6.1.1.d   Sample NAP-16: Garnet-bearing leucosome

Zircon morphology varies from subhedral to equant and euhedral, with a majority of grains having rounded edges (Fig. 6i). Grain size varies from 80–300 µm with a general aspect ratio of 1:2. CL imaging shows that the majority of grains display weakly to highly luminescent, poorly-zoned core surrounded by a darker overgrowth that ranges in width from 10–45 µm. Seventy-three analyses were obtained from 56 zircon grains with 36 rejected on the grounds of being <95% or >105% concordant or reversely discordant. There are two distinct ages clusters present in this sample (Fig.6d).The older population has a weighted average $^{207}Pb/^{206}Pb$ isotopic age of 1752 ± 15 Ma (n=18, MSWD= 1.7). The younger age cluster was analysed from darker CL overgrowths and gave $^{207}Pb/^{206}Pb$ unmix isotopic ages of 1634 ± 33 Ma (n=7, 36%) and 1596 ± 15 Ma (n=12, 64%) and a $^{207}Pb/^{206}Pb$ weighted average age of 1610 ± 13 Ma (n= 19, MSWD= 1.7); with Th/U ratios between 0.07 and 0.361. 0.006 and 0.065(fig 8d).The 1634 Ma ages are derived from analyses of overgrowths from predominantly sub-rounded grains with highly luminescent cores. A plot of Th/U ratio vs age for NAP-16 is shown in Fig.8d. The zircon analyses are characterised by a large range in Th/U values, and each age clustering is characterised by distinct Th/U ratios. The older ages are characterised by higher Th/U ratios ranging from 0.07 to 0.36, with most analyses clustering between about 0.07 and 0.20. A weak trend towards lower Th/U ratios with decreasing age is apparent for this age cluster. The younger ages are characterised by lower Th/U ranging from 0.006 to 0.065.

6.1.1.e   Sample 2012MR14:Granitic gneiss

Zircon grains vary in size from 100–200 µm and have a general 1:2 aspect ratio (Fig.6j).

CL imaging shows that the majority of zircons exhibit moderate luminescence and

moderately to well defined oscillatory zoning particularly within the cores, with thinner

darker homogeneous overgrowths present in most grains. Sixty analyses were obtained

from 52 zircon grains and 19 analyses were eliminated on the basis of being <95% and

>105% concordant. The age data indicated two age clusters (Fig.6e), with the majority

of data coming from zoned cores giving a single weighted average ^{207}Pb /^{206}Pb isotopic

age of 1774 ± 8 Ma (n=32, MSWD= 0.95), with concordancy between 95–105%.The

younger age grouping was obtained from darker overgrowths that were large enough to

accommodate a 30 µm spot. These analyses gave a weighted average ^{207}Pb /^{206}Pb

isotopic age of 1618 ± 34 Ma (n=7, MSWD= 2.6) (Fig.6e), with concordancy between

95–105%. A plot of Th/U ratio vs age for 2012MR14 is shown in Fig.8e. A large range

in Th/U values characterises the zircon analyses, from about 0.005 to 0.37. There is a

strong trend towards lower Th/U ratios with decreasing zircon age. Older zircon age

analyses are characterised by Th/U ratios for the cores ranged between 0.095 and 0.372.

By contrast, younger zircon age analyses are characterised by Th/U ratios ranging from

0.005 to 0.061.
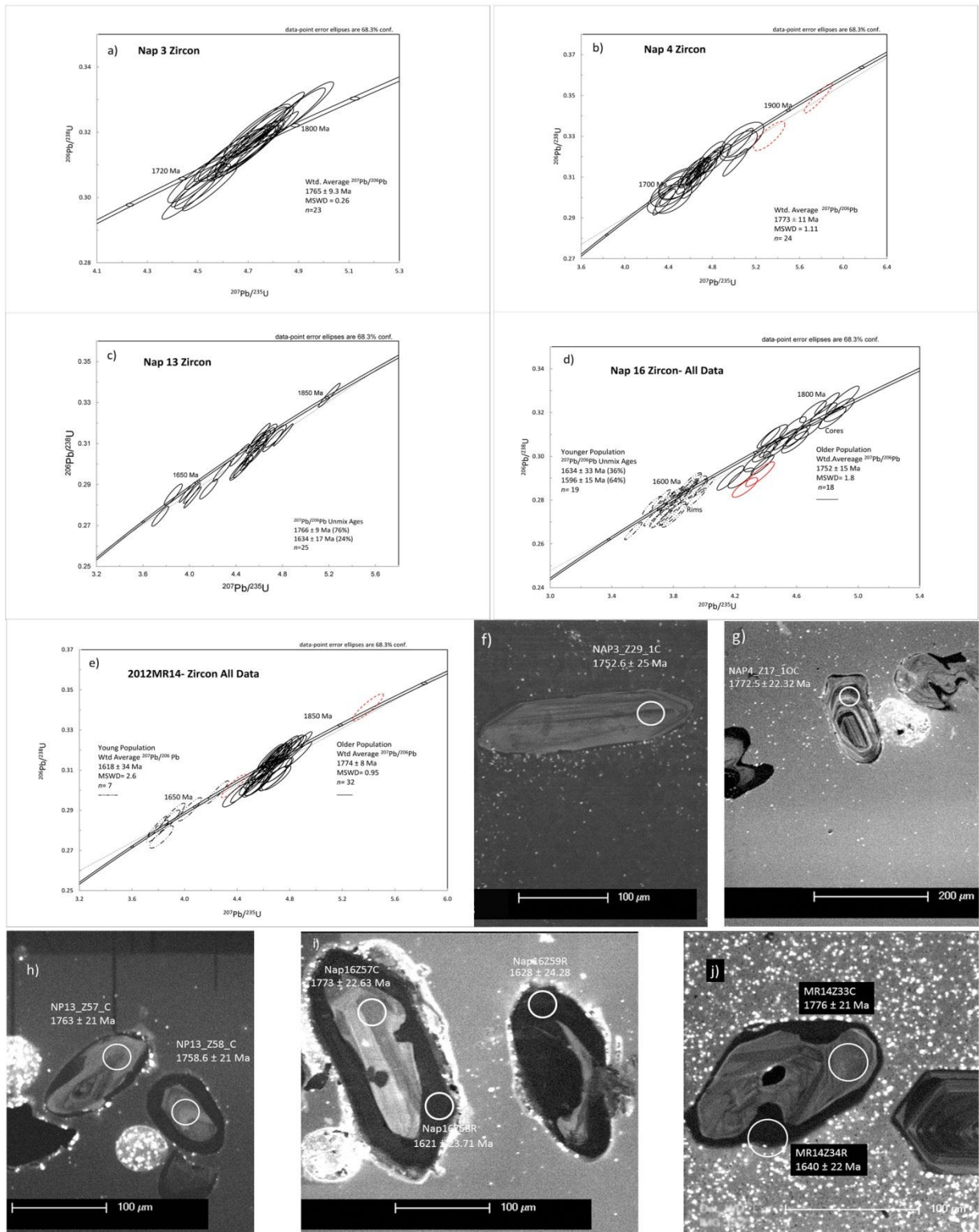
Figure 6: Concordia plots and CL images of magmatic interpreted samples a) NAP3: U-Pb Concordia plot with weighted ^{207}Pb /^{206}Pb isotopic age given. (b) NAP4: U-Pb Concordia plot with weighted ^{207}Pb /^{206}Pb isotopic age given. c) NAP13: U-Pb Concordia plot with unmix^{207}Pb /^{206}Pb isotopic ages given. d) NAP16: U-Pb Concordia plot with weighted ^{207}Pb /^{206}Pb and unmix isotopic ages given. e) 2012MR14: U-Pb Concordia plot with weighted ^{207}Pb /^{206}Pb isotopic age given. f) NAP3 euhedral zoned grain with^{207}Pb /^{206}Pb isotopic age given. g) NAP4 oscillatory zoned zircon

[207]Pb /[206]Pb isotopic age given. h) NAP13: Zircon with darker overgrowths- from leucosome [207]Pb /[206]Pb isotopic age given. i) NAP16: Zircon with darker overgrowths large enough to accommodate a 30μm beam[207]Pb /[206]Pb isotopic age given. j) 2012MR14: Zircon from the granitic gneiss with 2 fabrics [207]Pb /[206]Pb isotopic age given.

6.1.1.f   Sample 2012MR9: Sillimanite–cordierite–biotite metapelitic gneiss

Zircon grains varied in size from 50–120 μm and had a typical 1:3 aspect ratio (Fig.7f; g). CL imaging showed that the majority of grains exhibit moderate luminescence and moderately to well defined oscillatory zoning, particularly within the cores, with thinner darker homogeneous overgrowths present in most grains. Fifty-four analyses were obtained from 50 grains, with 11 being rejected on the basis of being <95% and >105% discordant.

There appear to be a large spread of ages with 7 peaks, but 5 main peaks starting from the oldest to youngest [207]Pb /[206]Pb clusters given with weighted average isotopic ages of, 2494 ± 21 Ma ($n=4$, MSWD=0.42) 2255 ± 54 Ma ($n=5$, MSWD=4.1), 2139 ± 39 Ma ($n=4$, MSWD=1.3), 1869 ± 24 Ma ($n=12$, MSWD=2.9) and 1761 ± 21 Ma ($n=14$, MSWD=2.5) Fig.7b; d. The weighted average for isotopic age 1761 ± 21 Ma is representative of the dominant peak and is largely from weakly luminescent, oscillatory zoned domains. A plot of Th/U ratio vs age for 2012MR9 is shown in Fig.8g. A large range in Th/U values characterises the zircon analyses, from about 0.03 to 0.78. Low Th/U ratios do not display a strong trend with younger ages.

6.1.1.g   Sample NAP-11a: Sillimanite–cordierite–biotite metapelitic gneiss

Zircon grains size varied from 50–150 μm and had a typical 1:2 aspect ratio (Fig.7e). CL imaging showed that the majority of grains exhibit moderate to subtle luminescence

and moderately- to well-defined oscillatory zoning, particularly within the cores, with darker homogeneous overgrowths common on euhedral grains. Seventy analyses were obtained from 64 grains, with 3 being rejected on the basis of being <95% or >105% concordant. There is a large spread of concordant ages providing a complex array of age peaks (Fig.7c), with 6 main peaks starting from the oldest to youngest ^{207}Pb $/^{206}Pb$ populations given with a weighted average isotopic ages of 2340 ± 33 Ma (n=10, MSWD=3.6), 2157 ± 32 Ma (n=7, MSWD=2.4), 2042 ± 23 Ma (n=9, MSWD=1.6), 1863 ± 20 Ma (n=25, MSWD=23), 1720 ± 22 Ma (n=4, MSWD= 0.80) and 1635 ± 20 Ma (n= 5, MSWD= 0.54) (Fig.6a; c). The weighted average for isotopic age 1863 ± 22 Ma is representative of the dominant peak and is largely from weakly luminescent, oscillatory zoned domains; 1720 ± 22 Ma is from weakly zoned darker overgrowths on euhedral grains. The youngest population of 1635 ± 20 Ma is given from darker overgrowths on euhedral grains. A plot of Th/U ratio vs age for NAP-11a is shown in Fig.8f. A large variation in Th/U ratios is evident, ranging from approximately 0 to 0.5. There is a subtle trend towards lower Th/U ratios for younger zircon ages.
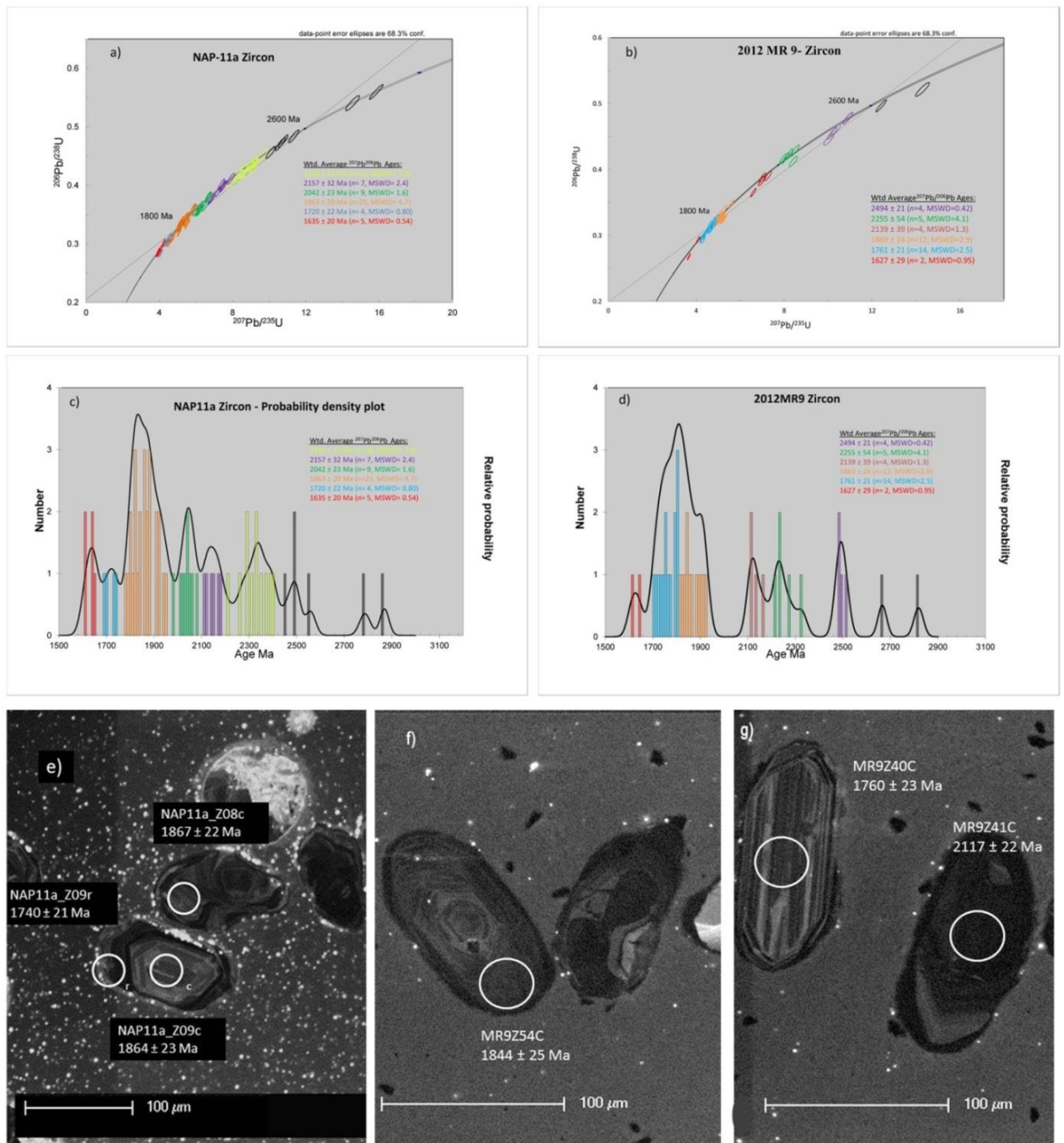
Figure 7: Concordia and Probability density plots along with Cl images of U-Pb zircon geochronology on the two metapelite samples. a & c) show colour coded concordia diagram and probability plot for NAP11a ages are weighted averages of clusters. b &d) show colour coded concordia diagram and probability plot for 2012MR9, ages are weighted averages of clusters. e) an example of zircons from a range of [207]Pb /[206]Pb isotopic ages for NAP11a. f &g) an example of zircons from a range of [207]Pb /[206]Pb isotopic ages for 2012MR9.
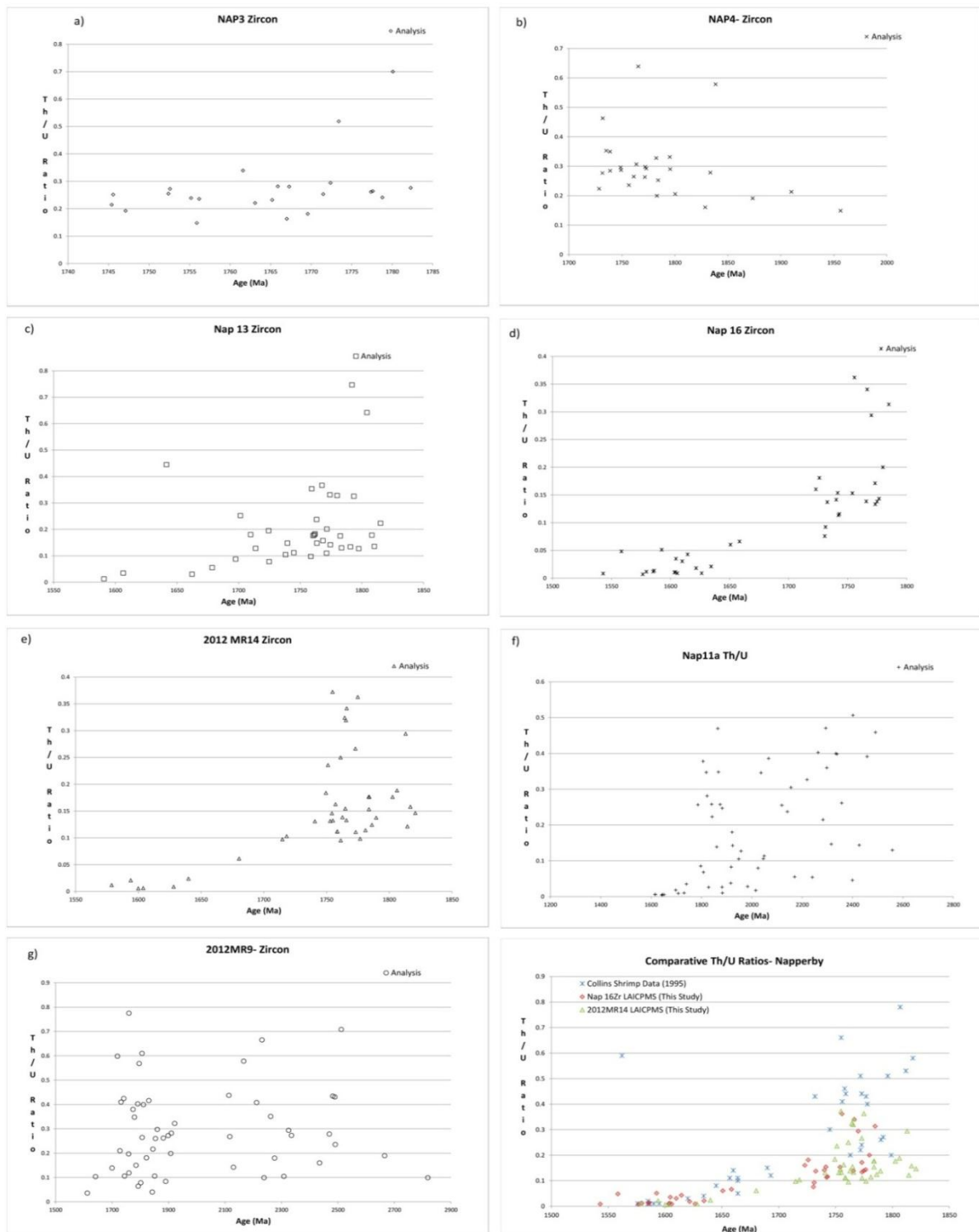
Figure 8: Calculated Th-U Ratio plots against age for all samples that had zircon analysis. Th/U ratios that are higher are often associated with magmatism and conversely those with lower ratios are often associated with recrystallization or metamorphism. The last Th\U plot is a comparative plot with data collected by Collins and Williams (1995) a larger copy is shown and discussed further in the text.

6.1.2 U-PB MONAZITE LA–ICP–MS GEOCHRONOLOGY

6.1.2.a   Sample NAP-4: Napperby Gneiss

Monazite grains were typically anhedral, rounded and cracked, and they varied in size from 50–150 µm (Fig.9e). Twenty-two analyses were obtained from 19 individual monazite grains. The spot analysis data for this sample is dominated by noisy time-resolved signals and high ^{204}Pb values. Eleven analyses were rejected on the basis of being outside ± 5% concordance and having elevated^{204}Pb values. The remaining data for this sample defines a spread of ages along concordia, this making it difficult to calculate weighted average ages with high degrees of certainty. Two^{207}Pb/^{206}Pb unmix isotopic ages of 1742 ± 16 Ma (*n*=7, 64%) and 1664 ± 23 Ma (*n*= 4, 36%) are defined (Fig.9a).

6.1.2.b   Sample NAP-13: Leucosome with retrogressed garnet

Monazite grains are dominated by anhedral shapes, 100–220 µm grain size and some indistinct zonation (Fig.9f). The grains are relatively unbroken and display pitting with the BSE detector. Twenty analyses were obtained from 19 grains and 3 analyses were rejected on the basis of being outside of ±5% concordance. A single weighted average ^{207}Pb/^{206}Pb isotopic age of 1555 ± 9 Ma (*n*=17, MSWD= 0.28) is defined (Fig.9b).

6.1.2.c   Sample 2012MR6: Garnet-absent leucosome

Monazite grains are anhedral, 50–200 µm in size and internal zoning is present in 5% of the imaged/analysed grains, zoning is apparent as faint rims as well as definitive darker cores. Twenty analyses were obtained from 18 individual monazite grains. Seven analyses were rejected on the basis of being outside ±5% concordance and one other

analysis was rejected in the calculations of weighted average by Isoplot. A single weighted average ^{207}Pb/^{206}Pb isotopic age of 1551 ± 14 Ma (*n*=12, MSWD= 1.2) is defined (Fig.9c).

6.1.2.d   Sample 2012MR14: Granitic gneiss

Monazite grains varied from anhedral to sub-rounded, ranged in size from 50–120 µm, were sparsely cracked and some zoning was visible on few grains as darker thin overgrowths with BSE imagery. Twenty analyses were conducted on 17 grains and all analyses fell within ±5% concordance. A single weighted average ^{207}Pb/^{206}Pb isotopic age of 1568 ± 9 Ma (*n*=20, MSWD= 0.49) is defined (Fig.9d).
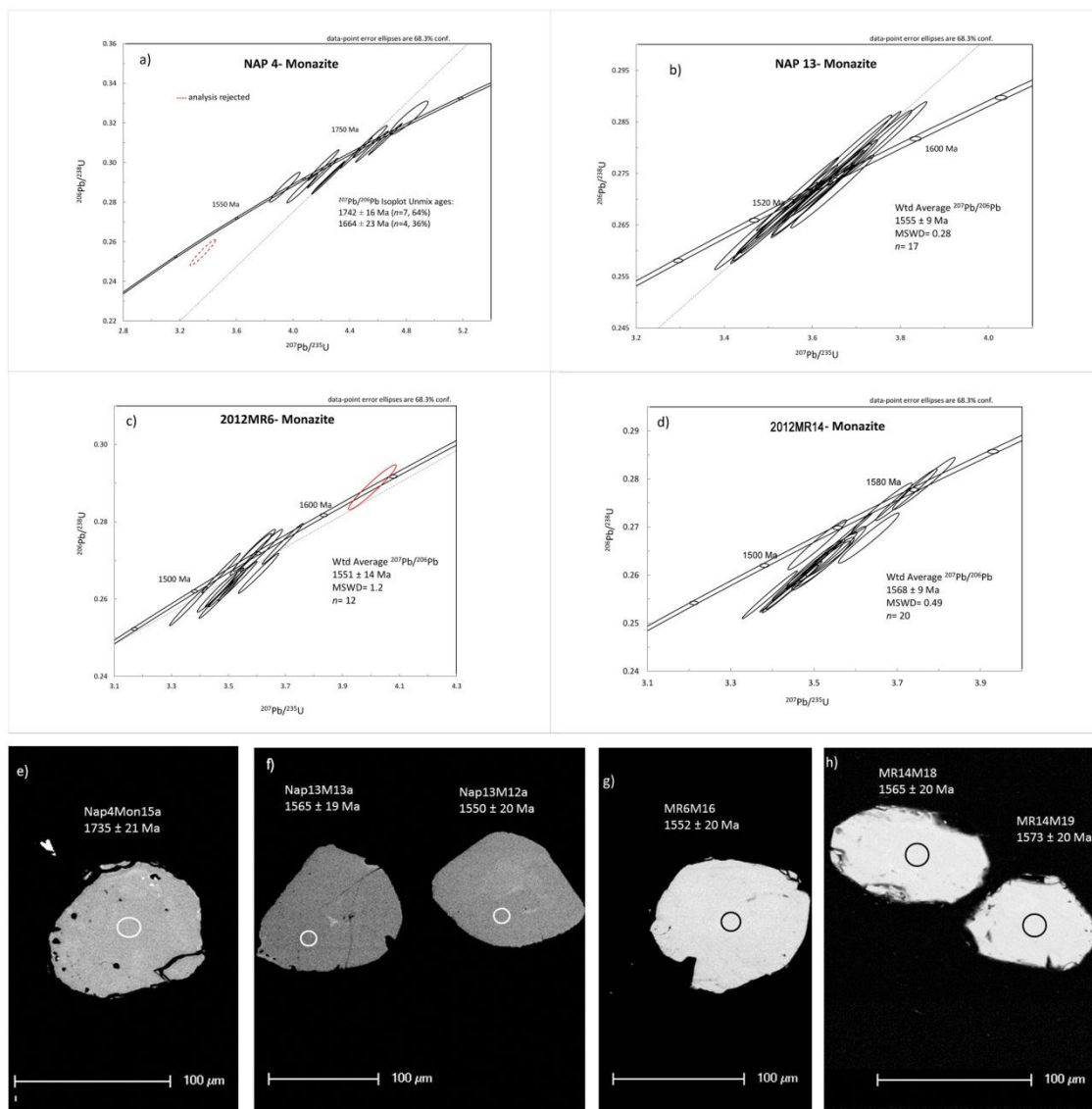
Figure 9: Concordia plots and BSE images of U-Pb monazite analysis. Red circles denote points that have been rejected on account of unreliability. a) NAP4 monazite concordia plot with unmix [207]Pb /[206]Pb isotopic ages b) NAP13: U-Pb Concordia plot with weighted [207]Pb /[206]Pb isotopic age given. c) 2012MR6 monazite: U-Pb Concordia plot with weighted [207]Pb /[206]Pb isotopic age given. d) 2012MR14 monazite: U-Pb Concordia plot with weighted [207]Pb /[206]Pb isotopic age given. e) NAP4 BSE image, [207]Pb /[206]Pb isotopic age f) NAP13 monazite,[207]Pb /[206]Pb isotopic age g) 2012MR6 monazite, [207]Pb /[206]Pb isotopic age h) 2012MR14 monazite [207]Pb /[206]Pb isotopic age.

6.1.2.e   Sample NAP-11a: Sillimanite–cordierite–biotite metapelitic gneiss

Monazite grains were predominantly anhedral with grain size ranging between 80–180 µm with some indistinct internal zonation. Twenty analyses were undertaken on 19 grains and 2 analyses were rejected on the basis of being outside ± 5% concordance.

Two $^{207}Pb/^{206}Pb$ unmix isotopic ages of 1621 ± 11 Ma (*n*=14, 76%) and 1547 ± 24 Ma (n=4, 24%) are defined (Fig.10a). Isoplot unmixing of the 1604 ± 19 Ma age was attempted since it does not correspond to any known tectonothermal event in the Arunta Complex.

6.1.2.f   Sample 2012MR9: Sillimanite–cordierite–biotite metapelitic gneiss

Monazite grains varied from anhedral to rounded, 50- 200 µm in size are commonly cracked and pitted and minimal zoning is revealed with BSE imagery. Twenty-four analyses were conducted on 19 grains with one analysis eliminated on the basis of being outside of ±5% concordance. A single weighted average $^{207}Pb/^{206}Pb$ isotopic age of 1556 ± 8 Ma (*n*=23, MSWD= 0.22) is defined (Fig.10b).

6.1.2.g   Sample 2012MR11: Sillimanite–cordierite–biotite metapelitic gneiss

Monazite grains exhibited anhedral morphology, ranged in size from 40 – 150 µm, were commonly cracked and no apparent zoning was revealed with BSE imagery. Twenty analyses were conducted on 19 grains and all analyses fell within ±5% concordance. A single weighted average $^{207}Pb/^{206}Pb$ isotopic age of 1557 ± 9 Ma (*n*=20, MSWD= 0.54) is defined (Fig.10c).
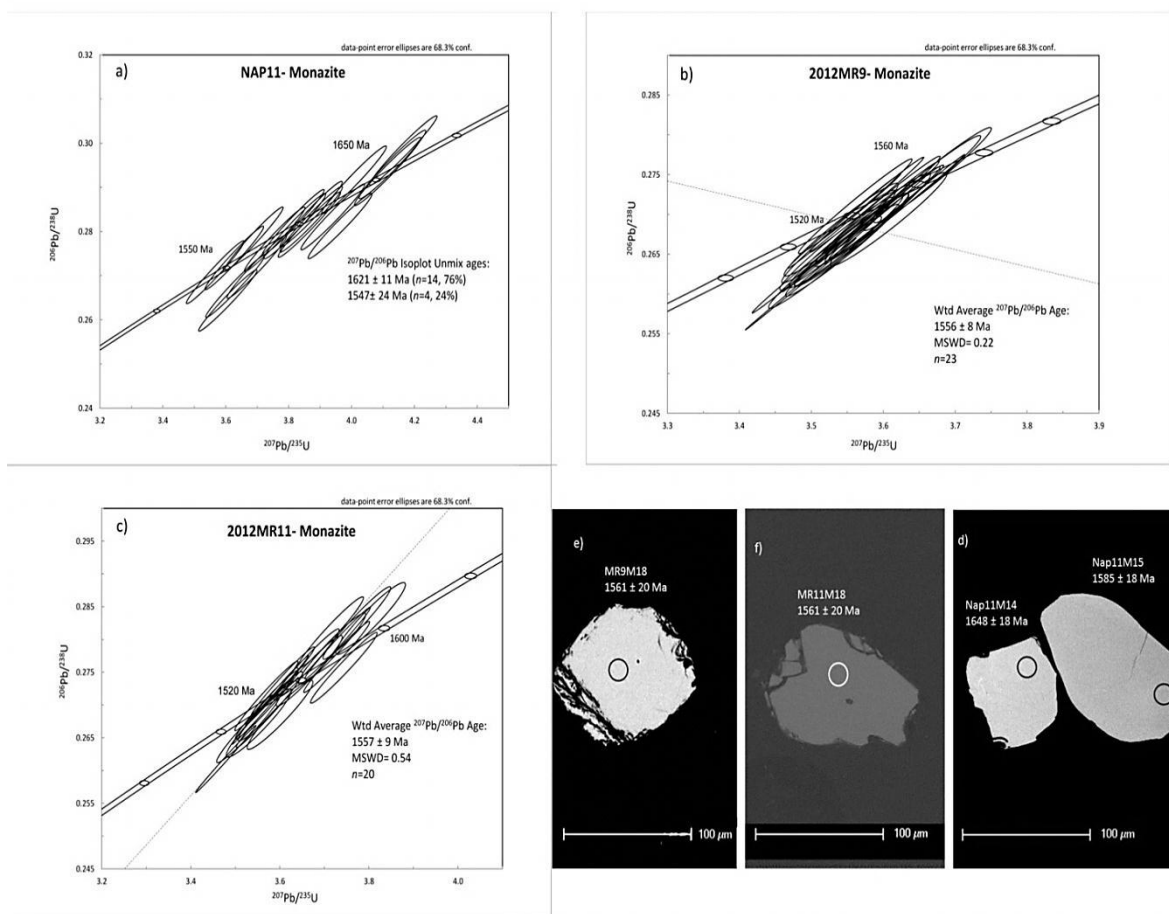
Figure 10: Concordia plots and BSE images for U-Pb monazites from metapelitic samples. a) NAP11a concordia diagram with unmix ^{207}Pb /^{206}Pb isotopic ages given. b) 2012MR9 concordia diagram with weighted ^{207}Pb /^{206}Pb isotopic age given. c) 2012MR11 concordia diagram with weighted ^{207}Pb /^{206}Pb isotopic age given. e) 2012MR9 monazite BSE image with ^{207}Pb /^{206}Pb isotopic age. f) 2012MR11 monazite BSE image with ^{207}Pb /^{206}Pb isotopic age. d) NAP11a monazite BSE image with ^{207}Pb /^{206}Pb isotopic age.

6.2 Petrography

Metapelitic sample 2012MR9 (Fig11a and 11b) was selected for metamorphic analysis

on the basis of having three visible fabrics as well as having zircon and monazite

available for geochronology. Medium- to coarse-grained biotite, sillimanite and quartz

are interpreted to define the early mineral assemblage. Sillimanite and biotite define the

S_3 fabric. Coarse cordierite commonly encloses/includes usually fine-grained sillimanite,

and these cordierite grains are interpreted to comprise part of the peak mineral

assemblage. Very coarse, twinned cordierite containing small, rounded inclusions of biotite and quartz occur in interpreted leucosomal domains in thin section.

The cordierite is also interpreted to comprise part of the peak assemblage. Rare coarser-grained sillimanite is not included (or near) cordierite, and therefore the peak mineral assemblage is interpreted to be cordierite + sillimanite + biotite + quartz (+/- K-feldspar +/- garnet). The interpreted consumption of some sillimanite by cordierite is the only potential evidence for peak to post-peak ('retrograde') mineral evolution. Rarely, some sillimanite and biotite grains are aligned at a low to moderate angle to the main gneissic fabric. The difference in alignment could reflect the two macroscopic fabrics S_3 and S_4.

Psammitic layers of sample 2012MR9 contain rare and small, rounded garnet grains in a quartz-rich matrix, a lower abundance of biotite (aligned to define S_3) and a low abundance of possible (twinned) cordierite grains. The psammitic layer is characteristically granoblastic by comparison to the metapelite.
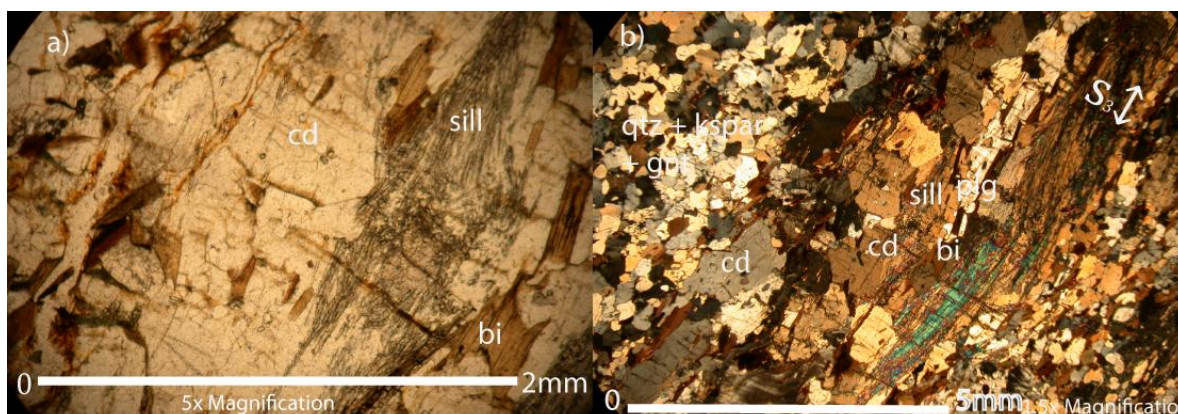
Figure 11: Photomicrographs of sample 2012MR9 a) Plain polarised light of fabric defining sillimanite and biotite, with cordierite enclosing fine grained sillimanite. b) Cross polarised light at 1.5 magnification showing granoblastic psammitic layer and S_3 fabric being defined by biotite and fine and coarse grained sillimanite.

6.2.1 PRESSURE-TEMPERATURE CONDITIONS

A pressure-temperature pseudosection was calculated for metapelite sample 2012MR9 (Fig.12) and presents a peak mineral assemblage at approximately 800-850°C and at pressures of approximately 4.5-6.5Kbar which is indicative of a high geothermal gradient of approximately >25-30 ^{o}C/Km. Previous work by (Buick *et al.* 1998) calculated pressure-temperature conditions of a metapelite within the Reynolds Range to be of similar values of 5Kbar and 750 - 850°C . A peak assemblage of K-feldspar, plagioclase, garnet, biotite, cordierite, sillimanite and quartz is consistent with the peak assemblage determined from petrographic observations. There is no definitive conclusion on the P-T path but could be decompressive based upon cordierite growth. The modelling for this sample is preliminary and is aimed at providing a generalised picture of the thermobarometric regime. Detailed thermobarometric modelling, compositional and P-T path matching is beyond the scope of this study.
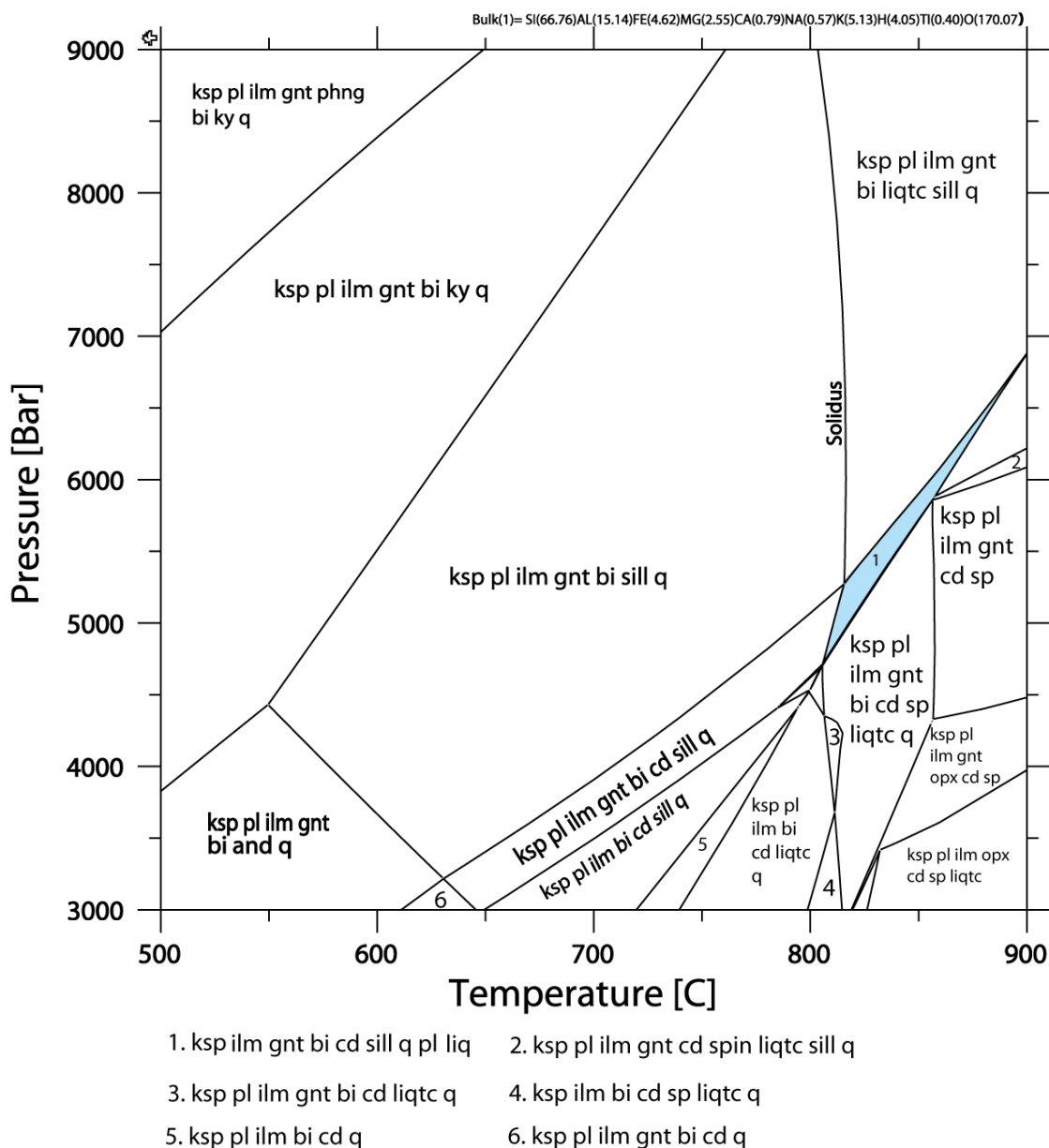
Figure 12: Pressure-temperature pseudosection for sample 2012MR9. Assemblage no.1 marked in blue denotes the peak assemblage of K-feldspar, ilmenite, garnet, biotite, cordierite, sillimanite, quartz, plagioclase and liquid Note P-T Pseudosection was calculated by A.Walsh. The modelling for this sample is preliminary and is aimed at providing a generalised picture of the pressure and temperature conditions of this rock.

7 DISCUSSION

The overarching aim of this study is to obtain (field) structurally constrained geochronological and metamorphic data with the aim of constraining the age of specific magmatic rocks, fabric elements and metamorphism, focussing on two regions in the Reynolds Range. The first region in the Woodforde River valley is characterised by existing geochronological data that is complex (Collins & Vernon 1991) that remains to be adequately explained in terms of event and tectonic significance. The second region, to the south of Mt Airyin the Yalyirimbi Range is part of a regionally extensive outcropping region of Napperby Gneiss for which there is no geochronological data. The data collected in this study directly contributes to addressing the larger questions about the tectonic significance of key event timelines in Proterozoic Australia.

7.1 INTERPRETATION OF GEOCHRONOLOGY

7.1.1 Zircon U-Pb Age Data

On the basis of all samples analysed for zircon U-Pb age data, there are clearly two age populations and/or clusters (Table 3). The older ages range between ca. 1775 and 1756 Ma and the younger ages range between ca. 1630 and 1596 Ma. The ca. 1775–1756 Ma ages are documented from Napperby Gneiss, mylonite in Napperby Gneiss and from garnet-bearing leucosomes as well as in the metapelite of 2012MR9. The younger ages (ca. 1630 Ma) are characterised by rim overgrowths on zircon grains in each of the two samples it was detected in (samples NAP-16 [garnet-bearing leucosome] and 2012MR14 [granitic gneiss]). Samples NAP-16 and 2012MR14 are both from the Woodforde River valley. This age does not match, but is broadly similar to, the ca. 1650 Ma U-Pb ages obtained by Collins and Williams (1995) from the same area for a

morphologically distinct population of multifaceted zircons that grew after the c. 1780 Ma magmatic population in the sampled granitic gneiss but before c. 1580 Ma overgrowths. Overgrowth age data for NAP-16 gave a weighted average age of 1604 ± 13 Ma.

The internal morphology of zircon in conjunction with plots of Th/U vs age may be used to aid in the interpretation of the zircon age data. In all samples except metapelitic gneiss 2012MR9, age data older than ca. 1700 Ma is characterised by Th/U ratios that would typically be interpreted as magmatic (e.g. Rubatto, 2002). Zircon age analyses with elevated Th/U ratios are typically characterised by oscillatory zoning, additionally attesting to the interpretation of magmatic origin.

On the basis of the age of 1773 ± 11 Ma obtained from NAP-4 it is interpreted to reflect the magmatic age of the Napperby Gneiss. Sample NAP-3 is also interpreted to preserve the magmatic age of the Napperby Gneiss and does not appear to record the age of low-grade mylonitisation.

The age data for leucosome samples NAP-13 (1766 ±9 Ma) and NAP-16 (1754±14 Ma) can be interpreted in two ways: the ages could reflect melting at this time or could reflect inheritance of old zircon during a younger melting event. Zircons from these leucosomes both had darker overgrowths that are interpreted as being metamorphic, while Nap 13 had rims that were too small to conduct analyses, Nap 16 had large overgrowths and a reasonable population of cores and rims were analysed.

These zircons are characterised by elevated Th/U ratios that may indicate inheritance rather than leucosome formation at this time. Both of these samples also have U-Pb monazite age data that needs to be considered in the interpretation, as discussed later. Figure 13, below shows a comparison of SHRIMPU-Pb data taken from Collins and Williams (1995) and data from NAP-16 and 2012MR14 (this study). A similar pattern is apparent between all three samples; lower Th/U ratios are evident from ca.1640 Ma, and in the case of both studies post ca.1640 Ma ages are representative of darker overgrowths on the zircon grains.
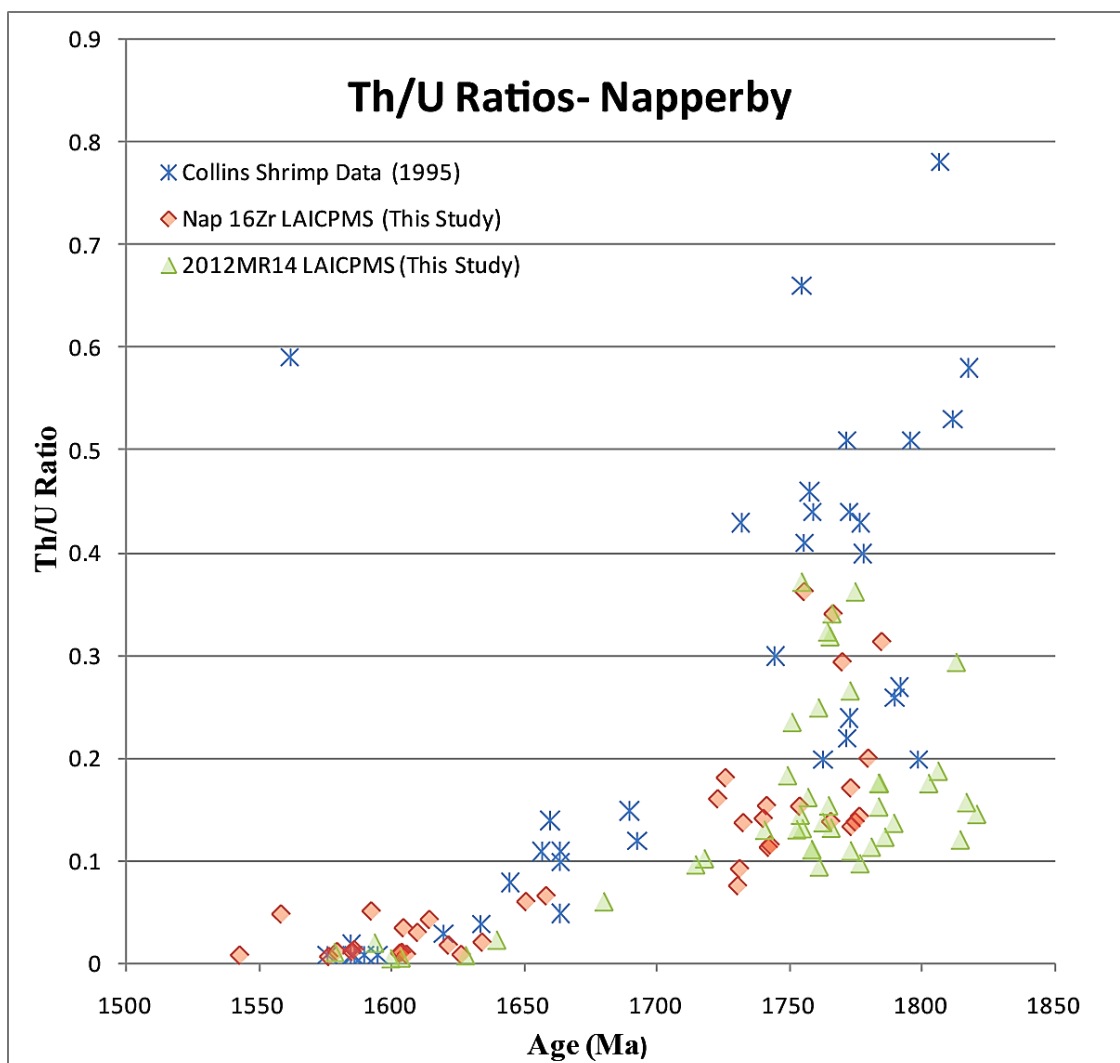
Figure 13: A comparison of Th/U ratios from Collins and Williams (1995) and this study. Lower Th/U ratios post 1640 Ma tend to be associated with darker overgrowths. NAP16 and 2012MR14 are samples which were collected for this study and are in close proximity to the sample collected by Collins and Williams (1995).

7.1.2 Maximum depositional ages of metapelitic rocks

U-Pb zircon age data from samples NAP-11a and 2012MR9 can be used to provide

constraint on the maximum depositional age of these metasediments. Plots of Th/U vs

age can also be helpful for this purpose.

Sample NAP-11a is characterised by an abundance of zircons with high Th/U ratios that

have ages ≥1786Ma. Thus, all such zircons can be interpreted as magmatic, and the

maximum depositional age for NAP-11a is approximately 1786 Ma. This result could mean that the metapelitic gneiss in the Yalyirimbi Range belongs to the Reynolds Range Group which is constrained to have been deposited between 1812 and 1785 Ma (Collins & Williams 1995, Williams *et al.* 1996). However, the youngest zircons in this sample have ages within analytical uncertainty of the minimum depositional age for the Lander Rock Beds (1806 Ma – Vry *et al*. 1996).

Sample 2012MR9 is characterised by an abundance of zircons with high (> ~0.14) Th/U ratios that have ages ≥1700 Ma (or thereabouts). Zircon with such elevated Th/U ratios would normally be interpreted as magmatic, however CL images of the c. 1700 Ma zircons appear dark and have no zoning which can be interpreted as being as that they are just recrystallising. Oscillatory zoning in zircon with little overgrowth appears from c.1720 Ma, which we think that this could mean that is a younger sequence with a maximum depositional age from c. 1720 Ma, which is contradictory to the previous constraints on the Reynolds Range Group of ca. 1812-1785 Ma (Collins & Williams 1995).

7.1.3 Monazite U-Pb Age Data

On the basis of all samples analysed for monazite U-Pb age data there is one clear age population and two far less distinct older age groups (see Table 3). The prominent age population encompasses the range ca. 1550 Ma to 1570 Ma and corresponds to the Chewings Event timeline (Hand & Buick 2001, Claoue-Long *et al.* 2008a). These ages are towards the younger end of the known/defined Chewings Event (Hand & Buick 2001) and thus may be interpreted to extend the known duration of the Chewings Event.

The older ages are only obtained through unmixing of age data (in Isoplot) and loosely define timelines at ca. 1620 Ma, 1664 Ma and 1742 Ma.

The monazite U-Pb age data corresponding to the Chewings Event is interpreted to reflect metamorphism at this time. The monazite data allows for interpretation of the zircon data in samples NAP-13 and NAP-16. The monazite age data indicate that the leucosomes formed during the Chewings Event and that zircon in these leucosomes is inherited from the host rock (Napperby Gneiss).Overall, the monazite age data indicate that high-grade, granulite-facies metamorphism of the studied portions of the Reynolds Range occurred during the Chewings Event (see also Rubatto et al. 2001; Williams et al. 1996; Vry et al. 1996).

7.1.4 Event timelines and fabric generations

Definitive timelines established in this study, namely ca. 1755–1775 Ma and ca. 1550–1570 Ma, correspond to known timelines of magmatism and metamorphism, respectively, in the Reynolds Range and Arunta Complex overall (Collins & Vernon 1991, Williams *et al.* 1996, Hand & Buick 2001, Scrimgeour 2003). On the basis of the relative structural framework for the Reynolds Range, summarised in Table 2, it seems likely that D_3/S_3 and D_4/S_4 both correspond to the Chewings Event. S_3 is the main penetrative fabric formed during D_3throughout the Reynolds Range, and its age is established by monazite geochronology from metapelitic rocks containing this fabric (NAP-11a and 2012MR9) and leucosomes of D_3 and D_4 generation. The age of the older fabric S2 is difficult to constrain directly as the S2 fabric is preserved only locally in F3 isoclinal hinges. The tectonic significance of the ca. 1620 Ma timeline, is only defined by a limited number of analyses, and is not possible to define here, and thus the

mystery of the broad timeline first defined by Collins and Williams et al. (1995) in the Woodforde River valley remains unclear. As such, it is not possible to constrainD_2/S_2, for example, to the ca. 1620 Ma timeline.

It may be that the ca. 1620–1650 Ma timeline is less evident in outcrop (structurally), just as it is geochronologically, that its significance was missed in the original structural framework proposed by Dirks & Wilson (1990). Nevertheless, in the southern Arunta Complex, Wong (2011), Fields (2012) and Lawson-Wyatt (2012) have identified magmatism and metamorphism corresponding to the ca. 1620–1640 Ma timeline. An absence of age populations corresponding to the Strangways Orogeny in this study most probably indicates that D2/S2 cannot be attributed to this event timeline. On the basis of present zircon age data the D2 event may closely correlate with the timing of magmatism and intrusion of the Napperby Gneiss.

7.1.5 Zircon vs monazite behaviour under high-grade conditions

Zircons are known to record magmatic recrystallization, but little new growth during high grade metamorphism or partial melting (Vry *et al.* 1996). Monazite is considered to break down during low T processes whilst tends to grow as a new metamorphic mineral during high grade metamorphism (Vry *et al.* 1996).Both of these minerals have high closure temperatures (Zr- >900°C, Mnz- >750°C) and are likely to record either metamorphic or magmatic events (Zeh *et al.* 2003).

Zircon is extremely useful and important for providing constraints on magmatism of older rocks (Watson 1996). Overgrowths on older zircon as seen in sample NAP-16 are

larger than those on 2012MR14 or NAP-13, and can provide cryptic clues as to the temperature of formation (Rubatto *et al.* 2001), with larger overgrowths representing higher temperatures (Rubatto *et al.* 2001) .

Monazite forms at lower temperatures than zircon (Vry *et al.* 1996, Rubatto *et al.* 2001, Zeh *et al.* 2003, Kelsey *et al.* 2008) , and can be highly susceptible to resetting and recrystallization in fluid present conditions (Kelly *et al.* 2012) .

The Chewings event was long lived and the Reynolds Range underwent slow cooling at ca. 1584 Ma following the peak of granulite facies metamorphism (Williams *et al.* 1996, Buick *et al.* 1998, Rubatto *et al.* 2001, Vry & Baker 2006) , and as a response to slow cooling monazite will record younger ages (Kelsey *et al.* 2008) . A reasonable explanation for the longevity of metamorphism and slow cooling is that there is high heat production sourced from the intruded granites that make up approximately 60% of the Reynolds Anmatjira Yalyirimbi Ranges (Loosveld 1989, Chamberlain & Sonder 1990, Buick *et al.* 1998, Sandiford & Hand 1998) .The age of mylonitisation could not be determined in this study, due to the sluggish response of zircon growth during high grade metamorphism or partial melting (Vry *et al.* 1996) . This opens up the speculation of D5 mylonitisation to be of either Chewings or Grenvillian since these are the last high grade, low-fluid events that occur in the aileron province before the Alice Springs Orogeny.

Table 3: Table of samples with their respective ages and interpretations. Samples NAP-3, NAP-4, NAP-11aare from south of Mt Airy. All other samples are from the Woodforde River valley.

Sample	GPS Coordinates	Description	Monazite age	MSWD	Interp.	Zircon age	MSWD	Interp.
NAP-3	291163 mE 7505462 mS	D_5mylonite in Napperby Gneiss				1765 ± 9 Ma	0.26	**Magmatic**
NAP-4	291187 mE 7505425 mS	Napperby Gneiss with planar S_3fabric	Isoplot Unmix ages : 1742 ± 16 Ma 1664 ± 23 Ma		Poor data, unclear interpretation	1773 ± 11 Ma	1.11	Magmatic
NAP-11a	304734 mE 7498708 mS	Sillimanite–cordierite–biotite metapelitic gneiss with S_3 fabric	Isoplot Unmix ages : 1621 ± 11 Ma 1547 ± 24 Ma		**2 metamorphic events**	Ca.1786 Ma (Max Dep)		Detrital
NAP-13	298804 mE 7511258 mS	D_4 leucosome with retrogressed garnet	1556 ± 9 Ma	0.26	**Metamorphic (Chewings)**	Isoplot Unmix ages : 1766 ± 9 Ma 1634 ± 17 Ma		Younger population most likely resetting Older population magmatic
NAP-16 Cores	299066 mE 7511254 mS	D_4 garnet-bearing leucosome				1752 ± 15 Ma	1.8	Magmatic- high Th/U ratio
NAP-16 Rims	299066 mE 7511254 mS	D_4 garnet-bearing leucosome				Unmix ages : Wtd Avge: 1634 ± 33Ma 1604 ± 13 Ma 1596 ± 15 Ma	1.7	**Metamorphic- low Th/U ratio**
2012MR6	299824 mE 7511466 mS	D_4 garnet-absent leucocratic melt	1555 ± 11 Ma	0.37	**Metamorphic (Chewings)**			
2012MR9	297926 mE 7512494 mS	Sillimanite–cordierite–biotite metapelitic gneiss. S_3 fabric on F_4 fold limb.	1556 ± 8 Ma	0.22	**Metamorphic (Chewings)**	Max Dep age is from ca.1760 Ma with a cluster of ages around 1860 Ma. Oldest grain 2800 Ma		Detrital
2012MR11	296866 mE 7514502 mS	Sillimanite–cordierite–biotite metapelitic gneiss fromF_3hinge. No zircons and a limited number of monazite available.	1558 ± 9 Ma	0.54	**Metamorphic (Chewings)**			
2012MR14	298051 mE 7511696 mS	Granitic gneiss with two fabrics (S_3 and S_4)	1569 ± 9 Ma	0.37	**Metamorphic (Chewings)**	2 Groups, tend to be separated by cores and a very small population of rims, rims are 1618 ± 34 Ma and Cores are at 1774 ± 8 Ma	2.6 and 0.95	Magmatic with a small number of metamorphic rims that could represent resetting of host zircons

8 CONCLUSIONS

This study has contributed U-Pb geochronological and metamorphic data that is invaluable to the growing data set that not only gives better local understanding of the Reynolds Anmatjira Yalyirimbi Ranges, but also contributes to underpinning larger-scale models of continental growth or assembly.

Samples that have been collected from a range of structural domains and fabric elements define two clear age populations, namely the Chewings (ca. 1570-1550) and Yambah-Inkamulla (1775-1755 Ma) events. Geochronology has also found a cryptic record of a possible event at ca.1630-1620 Ma. It is not clear on the basis of data collected in this study to constrain the tectonic significance of this timeline, but it may be that it is extensional based on new data obtained from the southern Arunta Province.

The majority of melting and deformation preserved in the field in the study area, and by inference, the high-grade SE end of Reynolds Range, is Chewings-aged. Two structurally distinct sets of leucosomes are the product of Chewings-aged tectonism.

New constraints on the deposition of Reynolds Range Group sediments have signified younger maximum depositional ages at ca.1786 Ma and possibly ca. 1760 Ma.

An understanding of event timelines has been achieved in this study by investigating carefully selected rocks within the Reynolds-Yalyirimbi Ranges. By analysing Zircon and monazite data along with assigning pressure-temperature constraints, it has been possible to provide constraints on magmatism, fabric elements and metamorphism.

9 ACKNOWLEDGMENTS

10 REFERENCES

BETTS P. G. & GILES D. 2006. The 1800-1100 Ma tectonic evolution of Australia. *Precambrian Research***144**, 92-125.

BLACK L. P. & SHAW R. D. 1992. U-PB ZIRCON CHRONOLOGY OF PROGRADE PROTEROZOIC EVENTS IN THE CENTRAL AND SOUTHERN PROVINCES OF THE ARUNTA BLOCK, CENTRAL AUSTRALIA. *Australian Journal of Earth Sciences***39**, 153-171.

BLACK L. P. & SHAW R. D. 1995. An assessment, based on U-Pb zircon data, of Rb-Sr dating in the Arunta Inlier, central Australia. *Precambrian Research***71**, 3-15.

BUICK I. S., CARTWRIGHT I. & HARLEY S. L. 1998. The retrograde P-T-t path for low-pressure granulites from the Reynolds Range, central Australia: petrological constraints and implications for low-P/high-T metamorphism. *Journal of Metamorphic Geology***16**, 511-529.

BUICK I. S., MILLER J. A., WILLIAMS I. S. & CARTWRIGHT I. 2001. Ordovician high-grade metamorphism of a newly recognised late Neoproterozoic terrane in the northern Harts Range, central Australia. *Journal of Metamorphic Geology***19**, 373-394.

C.E F. 2012. Liebig-aged (ca. 1640 Ma) magmatism and metamorphism in ca. 1760 Ma crust in the Warumpi and Southern Aileron Province, Central Australia: A case for revising the tectonic framework of Proterozoic Australia. Bsc Honours thesis, Geology and Geophysics, The University of Adelaide, Adelaide (unpubl.).

CARTWRIGHT I., BUICK I. S., FOSTER D. A. & LAMBERT D. D. 1999. Alice Springs age shear zones from the southeastern Reynolds Range, central Australia. *Australian Journal of Earth Sciences***46**, 355-363.

CAWOOD P. A. & KORSCH R. J. 2008. Assembling Australia: Proterozoic building of a continent. *Precambrian Research***166**, 1-35.

CHAMBERLAIN C. P. & SONDER L. J. 1990. Heat-producing elements and the thermal and baric patterns of metamorphic belts. *Science (New York, NY)***250**, 763.

CLAOUE-LONG J., EDGOOSE C. & WORDEN K. E. 2008a. A correlation of Aileron Province stratigraphy in central Australia. *Precambrian Research***166**, 230-245.

CLAOUE-LONG J., MAIDMENT D., HUSSEY K. & HUSTON D. L. 2008b. The duration of the Strangways Event in central Australia; evidence for prolonged deep crust processes. *Precambrian Research***166**, 246-262.

COGGON R. & HOLLAND T. J. B. 2002. Mixing properties of phengitic micas and revised garnet-phengite thermobarometers. *Journal of Metamorphic Geology***20**, 683-696.

COLLINS W. J. & SHAW R. D. 1995. Geochronological constraints on orogenic events in the Arunta Inlier; a review. *Precambrian Research***71**, 315-346.

COLLINS W. J. & VERNON R. H. 1991. Orogeny associated with anticlockwise P-T-t paths; evidence from low-P, high-T metamorphic terranes in the Arunta Inlier, central Australia. *Geology Boulder***19**, 835-838.

COLLINS W. J. & WILLIAMS I. S. 1995. SHRIMP ionprobe dating of short-lived Proterozoic tectonic cycles in the northern Arunta Inlier, central Australia. *Precambrian Research***71**, 69-89.

DIRKS P. & HAND M. 1991. Structural and metamorphic controls on the distribution of zircon in an evolving quartzofeldspathic migmatite; an example from the Reynolds Range, central Australia. *Journal of Metamorphic Geology***9**, 191-201.

DIRKS P. H. G. M., HAND M. & POWELL R. 1991. The P-T-deformation path for a mid-Proterozoic, low-pressure terrane; the Reynolds Range, central Australia. *Journal of Metamorphic Geology***9**, 641-661.

DIRKS P. H. G. M. & WILSON C. J. L. 1990. The geological evolution of the Reynolds Range, central Australia: evidence for three distinct structural-metamorphic cycles. *Journal of Structural Geology***12**, 651-665.

FLOTTMANN T. & HAND M. 1999. Folded basement-cored tectonic wedges along the northern edge of the Amadeus Basin, central Australia; evaluation of orogenic shortening. *Journal of Structural Geology***21**, 399-412.

GILES D., BETTS P. & LISTER G. 2002. Far-field continental backarc setting for the 1.80-1.67 Ga basins of northeastern Australia. *Geology Boulder***30**, 823-826.

GRIFFIN W. L., POWELL W. J., PEARSON N. J. & O'REILLY S. Y. 2008. *GLITTER: data reduction software for laser ablation ICP-MS. Laser Ablation ICP-MS in the Earth Sciences: Current Practices and Outstanding Issues., Mineralogical Association of Canada. Short Course Series 40*. Sylvester P.**:** 308-311.

HAND M. & BUICK I. S. 2001. Tectonic evolution of the Reynolds-Anmatjira ranges; a case study in terrain reworking from the Arunta Inlier, central Australia. *Geological Society Special Publications***184**, 237-260.

HAND M. & DIRKS P. H. G. M. 1992. The influence of deformation on the formation of axial-planar leucosomes and the segregation of small melt bodies within the migmatitic Napperby Gneiss, central Australia. *Journal of Structural Geology***14**, 591-604.

HAND M., MAWBY J., KINNY P. D. & FODEN J. 1999. U-Pb ages from the Harts Range, central Australia; evidence for early Ordovician extension and constraints on Carboniferous metamorphism. *Journal of the Geological Society of London***156, Part 4**, 715-730.

HOLLAND T. & POWELL R. 1998. An internally consistent thermodynamic data set for phases of petrological interest. *Journal of Metamorphic Geology***16**, 309-343.

HOLLAND T. & POWELL R. 2003. Activity–composition relations for phases in petrological calculations: an asymmetric multicomponent formulation. *Contributions to Mineralogy and Petrology***145**, 492-501.

JACKSON S. E., PEARSON N. J., GRIFFIN W. L. & BELOUSOVA E. A. 2004. The application of laser ablation-inductively coupled plasma-mass spectrometry to in situ U/Pb zircon geochronology. *Chemical Geology***211**, 47-69.

KELLY N. M., HARLEY S. L. & MOLLER A. 2012. Complexity in the behavior and recrystallization of monazite during high-T metamorphism and fluid infiltration. *Chemical Geology***322-323**, 192-208.

KELSEY D. E., CLARK C. & HAND M. 2008. Thermobarometric modelling of zircon and monazite growth in melt-bearing systems; examples using model metapelitic and metapsammitic granulites. *Journal of Metamorphic Geology***26**, 199-212.

LAFRANCE B., CLARKE G. L., COLLINS W. J. & WILLIAMS I. S. 1995. The emplacement of the Wuluma Granite; melt generation and migration along steeply dipping extensional fractures at the close of the late Strangways orogenic event, Arunta Block, central Australia. *Precambrian Research***72**, 43-67.

LOOSVELD R. J. H. 1989. The synchronism of crustal thickening and high T/low P metamorphism in the Mount Isa Inlier, Australia 1. An example, the central Soldiers Cap belt. *Tectonophysics***158**, 173-190.

M.A L.-W. 2012. Regional Inkamulla-aged (ca. 1740–1755 Ma) tectonism along strike of the Mt Hay-Redbank Hill region, southern Aileron Province, central Australia. Bsc Honours thesis, Geology and Geophysics, University of Adelaide Adelaide (unpubl.).

MAWBY, HAND& FODEN 1999. Sm–Nd evidence for high-grade Ordovician metamorphism in the Arunta Block, central Australia. *Journal of Metamorphic Geology***17**, 653-668.

MÖLLER A., HENSEN B. J., ARMSTRONG R. A., MEZGER K. & BALLÈVRE M. 2003. U-Pb zircon and monazite age constraints on granulite-facies metamorphism and deformation in the Strangways Metamorphic Complex (central Australia). *Contributions to Mineralogy and Petrology***145**, 406-423.

MORRISSEY L., PAYNE J. L., KELSEY D. E. & HAND M. 2011. Grenvillian-aged reworking in the North Australian Craton, central Australia, constraints from geochronology and modelled phase equilibria. *Precambrian Research***191**, 141-165.

RUBATTO D. 2002. Zircon trace element geochemistry; partitioning with garnet and the link between U-Pb ages and metamorphism. *Chemical Geology***184**, 123-138.

RUBATTO D., WILLIAMS I. S. & BUICK I. S. 2001. Zircon and monazite response to prograde metamorphism in the Reynolds Range, central Australia. *Contributions to Mineralogy and Petrology***140**, 458-468.

SANDIFORD M. & HAND M. 1998. Australian Proterozoic high-temperature, low-pressure metamorphism in the conductive limit. *Geological Society, London, Special Publications***138**, 109-120.

SANDIFORD M., HAND M. & MCLAREN S. 2001. Tectonic feedback, intraplate orogeny and the geochemical structure of the crust; a central Australian perspective. *Geological Society Special Publications***184**, 195-218.

SCRIMGEOUR I. 2003. Developing a revised framework for the Arunta region. *Geological Survey Record***001**, 2003-2001.

SCRIMGEOUR I. R., KINNY P. D., CLOSE D. F. & EDGOOSE C. J. 2005. High-T granulites and polymetamorphism in the southern Arunta region, central Australia; evidence for a 1.64 Ga accretional event. *Precambrian Research***142**, 1-27.

SHAW R. D., STEWART A. J. & BLACK L. P. 1984. The Arunta Inlier; a complex ensialic mobile belt in central Australia; Part 2, Tectonic history. *Australian Journal of Earth Sciences* **31**, 457-484.

SLAMA J., KOSLER J., CROWLEY J. L., GERDES A., HANCHAR J., HORSTWOOD M., MORRIS G. A., NASDALA L., NORBERG N., SCHALTEGGER U., TUBRETT M. N. & WHITEHOUSE M. J. 2007. Plesovice zircon; a new natural standard for U-Pb and Hf isotopic microanalysis. *Geochimica et Cosmochimica Acta* **71**, A947.

STEWART A. J. (Editor) 1981. *Reynolds Range region, Northern Territory*. Australian Government Publishing Service, Canberra, A.C.T., Australia.

VRY J., COMPSTON W. & CARTWRIGHT I. 1996. SHRIMP II dating of zircons and monazites; reassessing the timing of high-grade metamorphism and fluid flow in the Reynolds Range, northern Arunta Block, Australia. *Journal of Metamorphic Geology* **14**, 335-350.

VRY J. K. & BAKER J. A. 2006. LA-MC-ICPMS Pb/Pb dating of rutile from slowly cooled granulites; confirmation of the high closure temperature for Pb diffusion in rutile. *Geochimica et Cosmochimica Acta* **70**, 1807-1820.

WADE B. P., BAROVICH K. M., HAND M., SCRIMGEOUR I. R. & CLOSE D. F. 2006. Evidence for early Mesoproterozoic arc magmatism in the Musgrave Block, central Australia; implications for Proterozoic crustal growth and tectonic reconstructions of Australia. *Journal of Geology* **114**, 43-63.

WATSON E. B. 1996. Dissolution, growth and survival of zircons during crustal fusion; kinetic principles, geological models and implications for isotopic inheritance. *Special Paper Geological Society of America* **315**, 43-56.

WHITE R., POWELL R., HOLLAND T. & WORLEY B. 2000. The effect of TiO~ 2 and Fe~ 2O~ 3 on metapelitic assemblages at greenschist and amphibolite facies conditions: mineral equilibria calculations in the system K~ 2O-FeO-MgO-Al~ 2O~ 3-SiO~ 2-H~ 2O-TiO~ 2-Fe~ 2O~ 3. *Journal of Metamorphic Geology* **18**, 497-512.

WHITE R. W., POWELL R. & CLARKE G. L. 2002. The interpretation of reaction textures in Fe-rich metapelitic granulites of the Musgrave Block, central Australia: constraints from mineral equilibria calculations in the system K2O-FeO-MgO-Al2O3-SiO2-H2O-TiO2-Fe2O3. *Journal of Metamorphic Geology* **20**, 41-55.

WHITE R. W., POWELL R. & HOLLAND T. J. B. 2007. Progress relating to calculation of partial melting equilibria for metapelites. *Journal of Metamorphic Geology* **25**, 511-527.

WILLIAMS I. S., BUICK I. S. & CARTWRIGHT I. 1996. An extended episode of early Mesoproterozoic metamorphic fluid flow in the Reynolds Range, central Australia. *Journal of Metamorphic Geology* **14**, 29-47.

ZEH A., WILLIAMS I. S., BRAETZ H. & MILLAR I. L. 2003. Different age response of zircon and monazite during the tectono-metamorphic evolution of a high grade paragneiss from the Ruhla crystalline complex, central Germany. *Contributions to Mineralogy and Petrology* **145**, 691-706.

ZHAO J.-X. & MCCULLOCH M. T. 1995. Geochemical and Nd isotopic systematics of granites from the Arunta Inlier, central Australia; implications for Proterozoic crustal evolution. *Precambrian Research* **71**, 265-299.

APPENDIX A: U-PB LA-ICPMS ZIRCON DATA

Analysis	Ratios								Concordancy	Apparent ages (Ma)								Th/U Ratio
	$^{207}Pb/^{206}Pb$	1σ	$^{206}Pb/^{238}U$	1σ	$^{207}Pb/^{235}U$	1σ	$^{208}Pb/^{232}Th$	1σ		$^{207}Pb/^{206}Pb$	1σ	$^{206}Pb/^{238}U$	1σ	$^{207}Pb/^{235}U$	1σ	$^{208}Pb/^{232}Th$	1σ	
NAP-3 Mylonite																		
NAP3_Z03_1C	0.10681	0.00124	0.30938	0.00457	4.55508	0.07024	0.10159	0.00264	100	1745.6	21.08	1737.7	22.51	1741.1	12.84	1955.6	48.46	0.251133
NAP3_Z04_1C	0.10743	0.00127	0.30397	0.00451	4.50127	0.07013	0.09855	0.00268	97	1756.2	21.46	1710.9	22.28	1731.2	12.94	1899.8	49.36	0.235567
NAP3_Z05_1C	0.10898	0.0013	0.30275	0.0045	4.54797	0.07121	0.10188	0.00287	96	1782.3	21.66	1705	22.25	1739.8	13.03	1961	52.65	0.275616
NAP3_Z06_1R	0.10807	0.00138	0.30341	0.00456	4.51969	0.07338	0.0694	0.00221	97	1767	23.15	1708.2	22.53	1734.6	13.5	1356.1	41.84	0.162737
NAP3_Z07_1C	0.10689	0.0013	0.31191	0.00465	4.59584	0.07284	0.09887	0.00304	100	1747.1	22.04	1750.1	22.84	1748.5	13.22	1905.7	55.96	0.192111
NAP3_Z08_1C	0.10796	0.00133	0.30014	0.00448	4.46633	0.07129	0.09937	0.00316	96	1765.2	22.28	1692	22.22	1724.7	13.24	1914.9	58.18	0.231639
NAP3_Z09_1C	0.10839	0.00137	0.31659	0.00475	4.72997	0.0768	0.10378	0.00348	100	1772.4	22.97	1773	23.27	1772.6	13.61	1995.7	63.72	0.293843
NAP3_Z10_1C	0.10679	0.00145	0.30544	0.00464	4.49604	0.07589	0.0977	0.00352	98	1745.4	24.56	1718.2	22.91	1730.2	14.02	1884.1	64.88	0.214349
NAP3_Z11_1R	0.10869	0.0014	0.32543	0.00538	4.87682	0.08586	0.09173	0.00259	102	1777.6	23.33	1816.2	26.16	1798.3	14.84	1773.8	47.96	0.26385
NAP3_Z12_1R	0.10721	0.00138	0.31979	0.00529	4.72682	0.08317	0.09101	0.0026	102	1752.4	23.25	1788.7	25.82	1772	14.75	1760.6	48.15	0.254709
NAP3_Z13_1R	0.10741	0.00153	0.31305	0.00538	4.63591	0.08788	0.08491	0.00308	100	1755.9	25.76	1755.7	26.43	1755.8	15.83	1647.3	57.43	0.147651
NAP3_Z14_1R	0.10845	0.00139	0.31414	0.00519	4.69714	0.08283	0.06508	0.00197	99	1773.4	23.32	1761.1	25.43	1766.7	14.76	1274.3	37.33	0.518477
NAP3_Z15_1C	0.10869	0.0013	0.31443	0.00504	4.7117	0.07897	0.08769	0.00238	99	1777.4	21.75	1762.4	24.74	1769.3	14.04	1699	44.3	0.26119
NAP3_Z17_1R	0.10877	0.00142	0.32716	0.00547	4.90611	0.08808	0.09652	0.00319	103	1778.8	23.71	1824.6	26.57	1803.3	15.14	1862.3	58.8	0.241147
NAP3_Z19_1CD	0.108	0.00146	0.31529	0.00515	4.69491	0.0838	0.09718	0.00331	100	1765.9	24.56	1766.7	25.23	1766.3	14.94	1874.6	60.99	0.281508
NAP3_Z20_1C	0.10774	0.00146	0.31997	0.00516	4.75328	0.08424	0.09812	0.00337	102	1761.6	24.53	1789.6	25.21	1776.7	14.87	1891.8	61.98	0.339202
NAP3_Z21_1C	0.10783	0.00122	0.32029	0.00517	4.76152	0.07831	0.09466	0.00194	102	1763.1	20.54	1791.2	25.23	1778.1	13.8	1828	35.83	0.220705
NAP3_Z22_1R	0.10736	0.00129	0.32419	0.00536	4.79868	0.08234	0.09341	0.00238	103	1755.2	21.68	1810.2	26.08	1784.7	14.42	1805	44.03	0.238744
NAP3_Z23_1C	0.10885	0.00126	0.31843	0.00523	4.77842	0.0803	0.08997	0.00197	100	1780.1	20.94	1782.1	25.56	1781.1	14.11	1741.3	36.44	0.699971
NAP3_Z24_1C	0.10833	0.0012	0.31255	0.00504	4.66806	0.07607	0.08755	0.00182	99	1771.5	20.04	1753.3	24.74	1761.5	13.63	1696.3	33.81	0.252762

| Analysis | Ratios | | | | | | | | Concordancy | Apparent ages (Ma) | | | | | | | | Th/U Ratio |
	$^{207}Pb/^{206}Pb$	1σ	$^{206}Pb/^{238}U$	1σ	$^{207}Pb/^{235}U$	1σ	$^{208}Pb/^{232}Th$	1σ		$^{207}Pb/^{206}Pb$	1σ	$^{206}Pb/^{238}U$	1σ	$^{207}Pb/^{235}U$	1σ	$^{208}Pb/^{232}Th$	1σ	
NAP3_Z25_1R	0.10809	0.00156	0.31365	0.0055	4.67352	0.08947	0.06112	0.00204	100	1767.3	26.18	1758.6	27	1762.5	16.01	1199	38.81	0.279936
NAP3_Z28_1C	0.10822	0.00144	0.31576	0.00524	4.71106	0.08481	0.09527	0.0031	100	1769.6	24.13	1769	25.7	1769.2	15.08	1839.4	57.23	0.181113
NAP3_Z29_1C	0.10721	0.00148	0.32045	0.00538	4.73658	0.08732	0.09889	0.00328	99	1752.6	25.07	1791.9	26.27	1773.7	15.46	1906	60.28	0.272092
NAP-4 Napperby Gneiss with planar S$_3$ fabric																		
NAP4_Z01_1OC	0.10641	0.00308	0.3069	0.00502	4.50296	0.12908	0.08244	0.00824	99	1728.5	49.33	1705.6	24.03	1731.5	23.82	1601.1	153.9	0.349092
NAP4_Z03_1OC	0.10581	0.00289	0.30288	0.00486	4.4189	0.12046	0.07972	0.00744	97	1731.7	46.48	1688.3	23.4	1715.9	22.57	1550.3	139.26	0.223332
NAP4_Z04_1OC	0.10642	0.00283	0.30619	0.00488	4.49289	0.11958	0.08235	0.00742	98	1731.9	22.97	1703.6	21.03	1729.7	22.1	1599.5	138.58	0.284247
NAP4_Z05_1IC	0.106	0.00273	0.29939	0.00472	4.37612	0.11301	0.08016	0.007	97	1735.2	23.62	1680.3	20.99	1707.8	21.34	1558.6	131	0.276632
NAP4_Z07_1OC	0.10773	0.00265	0.29926	0.00467	4.44527	0.11059	0.07932	0.00651	99	1738.8	52.08	1725.4	24.77	1720.8	20.62	1542.8	122	0.264123
NAP4_Z09_1IC	0.1124	0.00243	0.32542	0.00485	5.04296	0.1125	0.08543	0.00619	99	1739	47.95	1721.9	24.09	1826.6	18.9	1656.9	115.22	0.57799
NAP4_Z12_1IC	0.11694	0.00184	0.33013	0.00471	5.32212	0.0946	0.09512	0.0043	100	1748.8	22.56	1755.9	21.68	1872.4	15.19	1836.5	79.34	0.21237
NAP4_Z12_1OC	0.11006	0.00167	0.31934	0.00449	4.84559	0.08299	0.09238	0.00382	100	1749.3	26.94	1751.2	22.56	1792.8	14.42	1785.9	70.72	0.205536
NAP4_Z13_1IC	0.11178	0.00258	0.32833	0.00568	5.07326	0.13094	0.05877	0.00384	99	1756.7	24.04	1747	21.75	1831.6	21.89	1154.3	73.24	0.15988
NAP4_Z14_1OC	0.10898	0.00152	0.31644	0.00441	4.75434	0.07704	0.08744	0.00311	96	1761.3	44.34	1687.6	23.19	1776.9	13.59	1694.3	57.84	0.32733
NAP4_Z15_1C	0.11209	0.00146	0.32712	0.00452	5.05514	0.07827	0.08994	0.00279	98	1763.7	24.42	1732.4	21.64	1828.6	13.12	1740.8	51.73	0.278283
NAP4_Z16_1C	0.10977	0.00156	0.31219	0.00446	4.72443	0.07823	0.08645	0.00302	99	1765.5	22.31	1756.4	21.6	1771.6	13.88	1675.9	56.26	0.289534
NAP4_Z17_1OC	0.10837	0.00133	0.31333	0.00429	4.68139	0.06968	0.08879	0.00245	99	1771.8	23.68	1753.5	21.77	1763.9	12.45	1719.4	45.54	0.297553
NAP4_Z18_1IC	0.12002	0.00144	0.34867	0.00478	5.76932	0.085	0.09637	0.00255	99	1772.1	22.32	1757.1	21.05	1750.3	14.44	1766	65.49	0.148211
NAP4_Z19_1OC	0.10702	0.00159	0.31213	0.00459	4.60557	0.07972	0.0913	0.00354	101	1773	27.88	1792.8	21.98	1783.6	14.48	1853.8	79.51	0.286907
NAP4_Z20_1OC	0.10842	0.00167	0.32063	0.0045	4.7926	0.0826	0.09606	0.00431	99	1782.4	25.33	1772.3	21.58	1783.6	14.48	1853.8	79.51	0.291974
NAP4_Z22_1OC	0.10909	0.00143	0.31819	0.00449	4.78558	0.0754	0.08412	0.00254	99	1783	22.08	1768.7	21.67	1782.4	13.23	1632.6	47.3	0.25217
NAP4_Z23_1C	0.10975	0.00146	0.30618	0.00434	4.63283	0.07351	0.07321	0.00215	100	1784.3	23.74	1780.9	21.96	1755.2	13.25	1428	40.49	0.330779
NAP4_Z24_1C	0.10601	0.00134	0.30248	0.00425	4.42065	0.06806	0.07085	0.00196	96	1795.3	23.98	1721.9	21.41	1716.2	12.75	1383.5	37.04	0.462444
NAP4_Z27_1C	0.10902	0.00133	0.31571	0.00442	4.74507	0.07156	0.08175	0.00212	98	1795.6	25.7	1751.5	21.9	1775.2	12.65	1588.2	39.57	0.199341
NAP4_Z31_1OC	0.11459	0.00138	0.31719	0.00445	5.01091	0.07494	0.10562	0.00266	99	1800.4	27.39	1786.5	21.94	1821.2	12.66	2029.5	48.63	0.190809

Analysis	Ratios								Concordancy	Apparent ages (Ma)								Th/U Ratio
	$^{207}Pb/^{206}Pb$	1σ	$^{206}Pb/^{238}U$	1σ	$^{207}Pb/^{235}U$	1σ	$^{208}Pb/^{232}Th$	1σ		$^{207}Pb/^{206}Pb$	1σ	$^{206}Pb/^{238}U$	1σ	$^{207}Pb/^{235}U$	1σ	$^{208}Pb/^{232}Th$	1σ	
NAP4_Z32_1OC	0.10699	0.00133	0.3131	0.00442	4.61844	0.0705	0.07937	0.00206	100	1828.6	41.19	1830.3	27.58	1752.6	12.74	1543.8	38.65	0.295957
NAP4_Z34_1OC	0.1062	0.00138	0.29778	0.00423	4.36012	0.0682	0.08029	0.00221	99	1833.6	23.37	1824.4	21.98	1704.8	12.92	1561.1	41.37	0.352064
NAP4_Z24_2OC	0.10798	0.00133	0.31319	0.0044	4.6622	0.07065	0.07881	0.00217	99	1838.5	38.67	1816.1	23.57	1760.5	12.67	1533.3	40.61	0.638617
NAP4_Z36_1C	0.10835	0.00141	0.3126	0.00443	4.66966	0.07333	0.08121	0.00246	95	1873.4	21.52	1776	21.78	1761.8	13.13	1578.1	46.05	0.262721
NAP4_Z37_1OC	0.10746	0.00143	0.31128	0.00442	4.61148	0.07321	0.07851	0.00248	96	1909.9	28.03	1839	22.83	1751.3	13.25	1527.6	46.51	0.235467
NAP4_Z38_1OC	0.10787	0.00146	0.30831	0.00439	4.58493	0.07353	0.0764	0.00248	99	1956.5	21.26	1928.2	22.86	1746.5	13.37	1488	46.6	0.306675
NAP-13 D4 leucosome with retrogressed garnet									-									
NP13Z39R	0.09824	0.00118	0.28509	0.00342	3.86045	0.05147	0.08956	0.00282	102	1590.9	22.27	1616.9	17.16	1605.5	10.75	1733.7	52.23	0.012158
NP13Z36C	0.09907	0.00114	0.27452	0.00323	3.74876	0.04802	0.08304	0.00215	97	1606.6	21.36	1563.7	16.36	1581.8	10.27	1612.4	40.14	0.034478
NP13Z5R	0.09919	0.00104	0.2727	0.00314	3.72793	0.04396	0.10129	0.00174	97	1608.9	19.41	1554.5	15.89	1577.4	9.44	1950.2	32.02	0.147583
NP13Z3C	0.10095	0.00107	0.28629	0.0033	3.98305	0.0474	0.01158	0.00019	99	1641.6	19.59	1623	16.54	1630.7	9.66	232.6	3.85	0.444184
NP13Z21R	0.10208	0.0011	0.28572	0.00328	4.02133	0.04818	0.159	0.00307	97	1662.3	19.84	1620.1	16.43	1638.5	9.74	2982.4	53.59	0.029803
NP13Z19C	0.10298	0.00108	0.28367	0.0034	4.02662	0.04952	0.09138	0.00146	96	1678.6	19.32	1609.8	17.09	1639.6	10	1767.4	27.09	0.054877
NP13Z41C	0.10474	0.00116	0.29651	0.00334	4.28078	0.05116	0.09164	0.00173	98	1709.8	20.16	1674	16.61	1689.7	9.84	1772.3	31.98	0.17959
NP13Z52C	0.10498	0.00121	0.28779	0.00322	4.16527	0.05109	0.09188	0.00221	95	1714	21.08	1630.5	16.1	1667.2	10.04	1776.7	40.88	0.127562
NP13Z24C	0.10558	0.00115	0.30439	0.00357	4.43094	0.05443	0.09461	0.0017	99	1724.4	19.89	1713	17.64	1718.1	10.18	1827.1	31.48	0.194459
NP13Z26C	0.10638	0.00115	0.31431	0.00368	4.6099	0.05644	0.09763	0.00181	101	1738.2	19.73	1761.9	18.07	1751.1	10.22	1882.9	33.38	0.103788
NP13Z53C	0.10677	0.0012	0.31045	0.00339	4.56967	0.05403	0.10112	0.00226	100	1745	20.48	1742.9	16.69	1743.8	9.85	1946.9	41.46	0.111522
NP13Z58C	0.10757	0.00126	0.30917	0.00339	4.58485	0.05573	0.09276	0.00233	99	1758.6	21.15	1736.6	16.69	1746.5	10.13	1792.9	43.03	0.097049
NP13Z62C	0.10762	0.00123	0.31101	0.0035	4.61446	0.0562	0.08947	0.00176	99	1759.4	20.62	1745.7	17.23	1751.9	10.16	1732.1	32.69	0.353362
NP13Z54C	0.10768	0.0013	0.31415	0.00354	4.66373	0.05927	0.09917	0.00268	100	1760.6	21.81	1761.1	17.39	1760.8	10.63	1911.1	49.3	0.175606
NP13Z18R	0.10777	0.00114	0.29804	0.00346	4.42801	0.05289	0.09051	0.00126	95	1762.1	19.14	1681.6	17.21	1717.6	9.89	1751.2	23.31	0.182439
NP13Z57C	0.10785	0.00125	0.31264	0.0034	4.64857	0.05581	0.08964	0.00216	99	1763.4	20.93	1753.7	16.71	1758	10.03	1735.1	40.14	0.237002
NP13Z67C	0.10811	0.00124	0.29717	0.00335	4.4291	0.05457	0.08365	0.00195	95	1767.7	20.85	1677.3	16.64	1717.8	10.21	1623.7	36.4	0.366399
NP13Z31C	0.10815	0.00127	0.30534	0.00371	4.55238	0.06041	0.09395	0.00241	97	1768.5	21.33	1717.7	18.34	1740.6	11.05	1814.9	44.55	0.156954

Analysis	Ratios								Concordancy	Apparent ages (Ma)								Th/U Ratio
	$^{207}Pb/^{206}Pb$	1σ	$^{206}Pb/^{238}U$	1σ	$^{207}Pb/^{235}U$	1σ	$^{208}Pb/^{232}Th$	1σ		$^{207}Pb/^{206}Pb$	1σ	$^{206}Pb/^{238}U$	1σ	$^{207}Pb/^{235}U$	1σ	$^{208}Pb/^{232}Th$	1σ	
NP13Z29C	0.10833	0.00122	0.29872	0.00356	4.46139	0.05662	0.09191	0.00199	95	1771.5	20.47	1684.9	17.66	1723.8	10.53	1777.2	36.9	0.109321
NP13Z2C	0.10849	0.00116	0.30215	0.00348	4.51913	0.0537	0.08826	0.00117	96	1774.2	19.36	1701.9	17.2	1734.5	9.88	1709.5	21.79	0.330445
NP13Z65C	0.10851	0.00125	0.30459	0.00348	4.55661	0.05667	0.08921	0.00204	97	1774.5	20.84	1714	17.19	1741.4	10.36	1727.3	37.89	0.141384
NP13Z69C	0.10965	0.00133	0.31367	0.00362	4.74173	0.06146	0.09351	0.00233	98	1793.6	21.89	1758.8	17.75	1774.6	10.87	1806.9	43.03	0.324598
NP13Z28C	0.10989	0.00122	0.31146	0.00363	4.71878	0.05815	0.09304	0.00184	97	1797.6	20.04	1747.9	17.84	1770.6	10.33	1798.1	34.11	0.126715
NP13Z20C	0.11096	0.00115	0.31423	0.00361	4.80692	0.05619	0.09263	0.0012	97	1815.2	18.72	1761.5	17.69	1786.1	9.83	1790.6	22.23	0.223004
NAP-16 Garnet bearing leucosome																		
45R	0.09748	0.00104	0.27928	0.00279	3.75418	0.03955	0.09247	0.0022	101	1576.5	19.87	1587.7	14.08	1583	8.45	1787.5	40.76	0.006823
29R	0.09575	0.00109	0.2775	0.00283	3.66357	0.04126	0.06863	0.00189	102	1542.9	21.22	1578.8	14.3	1563.5	8.98	1341.6	35.8	0.008116
67R	0.10012	0.00115	0.2736	0.00346	3.77686	0.0513	0.21394	0.00572	96	1626.4	21.26	1559	17.53	1587.8	10.9	3918.6	95.2	0.00868
66R	0.09902	0.00113	0.28437	0.00359	3.88254	0.05252	0.13866	0.00381	100	1605.8	21.21	1613.3	18.03	1610.1	10.92	2624.6	67.62	0.008786
71R	0.09889	0.0013	0.27879	0.00368	3.80112	0.05744	0.08919	0.00338	99	1603.3	24.31	1585.3	18.56	1593	12.15	1726.9	62.69	0.010129
5R	0.09893	0.0011	0.28731	0.00296	3.91789	0.04357	0.12089	0.00289	102	1604	20.55	1628.1	14.8	1617.4	9	2306.7	52.14	0.010848
48R	0.09765	0.00104	0.27229	0.00273	3.66634	0.03863	0.12669	0.00246	98	1579.6	19.84	1552.4	13.82	1564.1	8.41	2411	44.21	0.011496
65R	0.09794	0.0011	0.28016	0.00355	3.78306	0.05086	0.09349	0.00237	100	1585.3	20.9	1592.2	17.9	1589.2	10.8	1806.5	43.85	0.011702
61R	0.09798	0.00125	0.28064	0.00356	3.7916	0.05477	0.08965	0.00309	101	1586.1	23.62	1594.6	17.9	1591	11.61	1735.4	57.27	0.013458
58R	0.09987	0.00128	0.28544	0.00368	3.93033	0.0579	0.10108	0.00349	100	1621.6	23.71	1618.7	18.48	1619.9	11.92	1946.3	64.11	0.017948
56R	0.10055	0.00127	0.27388	0.00358	3.79653	0.05592	0.0907	0.003	95	1634.3	23.32	1560.5	18.11	1592	11.84	1754.8	55.51	0.020753
55R	0.09924	0.00116	0.27255	0.00347	3.72889	0.05125	0.08111	0.00222	97	1609.9	21.69	1553.7	17.56	1577.6	11	1576.2	41.44	0.030243
27R	0.09896	0.00112	0.27187	0.00278	3.70944	0.04159	0.08925	0.00204	97	1604.6	20.96	1550.3	14.07	1573.4	8.97	1728	37.86	0.034767
6C	0.09948	0.00111	0.28225	0.00291	3.8703	0.04312	0.08439	0.00184	99	1614.4	20.56	1602.7	14.61	1607.5	8.99	1637.5	34.23	0.042808
46R	0.09655	0.00104	0.26593	0.00266	3.54036	0.03744	0.03093	0.00063	98	1558.5	20.02	1520.1	13.55	1536.3	8.37	615.6	12.26	0.048186
24R	0.09832	0.00111	0.28053	0.00287	3.80268	0.04247	0.07289	0.00161	100	1592.5	20.86	1594	14.45	1593.3	8.98	1422	30.34	0.051066
43R	0.10145	0.0011	0.28622	0.00289	4.00376	0.04281	0.08074	0.00146	98	1650.8	19.93	1622.6	14.46	1635	8.69	1569.3	27.36	0.060252
47R	0.10187	0.00111	0.28121	0.00284	3.95005	0.04234	0.10158	0.00184	97	1658.4	19.97	1597.5	14.28	1624	8.68	1955.5	33.79	0.065937

Analysis	Ratios								Concordancy	Apparent ages (Ma)								Th/U Ratio
	$^{207}Pb/^{206}Pb$	1σ	$^{206}Pb/^{238}U$	1σ	$^{207}Pb/^{235}U$	1σ	$^{208}Pb/^{232}Th$	1σ		$^{207}Pb/^{206}Pb$	1σ	$^{206}Pb/^{238}U$	1σ	$^{207}Pb/^{235}U$	1σ	$^{208}Pb/^{232}Th$	1σ	
40R	0.10593	0.00145	0.29755	0.00307	4.34542	0.057	0.09611	0.00353	97	1730.6	24.9	1679.1	15.27	1702	10.83	1854.8	65.08	0.0757
39C	0.10598	0.00141	0.29008	0.00304	4.23833	0.05481	0.09256	0.00313	95	1731.3	24.14	1641.9	15.19	1681.5	10.62	1789.2	57.96	0.092234
35C	0.10661	0.00135	0.30397	0.00314	4.46783	0.05512	0.09149	0.00271	98	1742.2	23.01	1711	15.55	1725	10.24	1769.4	50.16	0.113089
23C	0.10665	0.0012	0.30772	0.00316	4.52465	0.05068	0.08548	0.00178	99	1742.9	20.49	1729.5	15.58	1735.5	9.31	1657.9	33.18	0.115505
12C	0.10845	0.00134	0.31928	0.0034	4.77302	0.05897	0.09231	0.00253	101	1773.4	22.4	1786.2	16.6	1780.2	10.37	1784.5	46.81	0.133296
16C	0.10606	0.00131	0.31302	0.00333	4.57643	0.05702	0.08824	0.00254	101	1732.7	22.55	1755.6	16.37	1745	10.38	1709.2	47.24	0.137056
38C	0.10854	0.00141	0.31249	0.00324	4.67604	0.05885	0.08709	0.00272	99	1774.9	23.48	1752.9	15.92	1763	10.53	1687.8	50.63	0.138004
26C	0.10799	0.00125	0.30834	0.00318	4.59079	0.05266	0.08564	0.0019	98	1765.7	21.06	1732.5	15.67	1747.6	9.56	1660.9	35.45	0.138176
10C	0.1065	0.00124	0.32265	0.00336	4.73647	0.05508	0.0878	0.00208	104	1740.3	21.25	1802.7	16.35	1773.7	9.75	1701	38.66	0.141141
18C	0.10863	0.00134	0.30649	0.00327	4.58976	0.05727	0.09795	0.00286	97	1776.5	22.39	1723.4	16.15	1747.4	10.4	1888.7	52.66	0.143234
7C	0.1073	0.00122	0.29609	0.00306	4.379	0.04968	0.09045	0.00198	95	1754	20.6	1671.9	15.21	1708.4	9.38	1750.2	36.66	0.153053
34C	0.10656	0.00132	0.3204	0.0033	4.70737	0.05713	0.09113	0.00258	103	1741.5	22.51	1791.7	16.13	1768.6	10.16	1762.8	47.85	0.153689
31C	0.1055	0.00132	0.30209	0.00308	4.3939	0.05336	0.09022	0.00261	99	1723.1	22.88	1701.7	15.27	1711.2	10.05	1745.9	48.38	0.160208
50C	0.10567	0.00118	0.3042	0.00308	4.43248	0.0487	0.09253	0.00162	99	1726	20.4	1712.1	15.24	1718.4	9.1	1788.7	29.99	0.180792
53C	0.10913	0.00134	0.3257	0.0042	4.90063	0.06977	0.09431	0.00253	102	1784.9	22.24	1817.5	20.44	1802.4	12.01	1821.5	46.78	0.313285
2C	0.10805	0.00124	0.30946	0.0032	4.6085	0.05236	0.09628	0.00192	98	1766.6	20.79	1738	15.75	1750.8	9.48	1857.9	35.35	0.340269
42C	0.1074	0.00121	0.32403	0.00329	4.79868	0.053	0.08749	0.00148	99	1755.7	20.38	1809.4	16.03	1784.7	9.28	1695.2	27.49	0.361972
2012MR14 Granitic Gneiss with 2 fabrics																		
MR14Z19RC	0.09872	0.00122	0.28794	0.00368	3.91909	0.05585	0.08642	0.0032	102	1600	22.9	1631.2	18.44	1617.6	11.53	1675.4	59.59	0.005625
MR14Z41RC	0.09892	0.0012	0.28459	0.00366	3.88113	0.05503	0.10119	0.00356	101	1603.9	22.49	1614.4	18.38	1609.8	11.45	1948.4	65.27	0.006292
MR14Z24R	0.10022	0.00139	0.27673	0.00368	3.82422	0.05989	0.16682	0.00663	97	1628.2	25.53	1574.9	18.59	1597.9	12.6	3118.5	114.85	0.008611
MR14Z29R	0.0976	0.00107	0.28168	0.00357	3.79003	0.04994	0.09395	0.00234	101	1578.8	20.37	1599.8	17.93	1590.6	10.59	1814.9	43.29	0.011804
MR14Z44R	0.09839	0.00122	0.27958	0.00363	3.79232	0.05471	0.0596	0.00196	100	1593.9	22.98	1589.2	18.27	1591.1	11.59	1170.2	37.31	0.020742
MR14Z34R	0.10085	0.00124	0.29047	0.00385	4.03893	0.05902	0.08773	0.00282	100	1639.9	22.64	1643.9	19.24	1642.1	11.89	1699.7	52.32	0.023741
MR14Z9R	0.10308	0.00117	0.29894	0.00381	4.24853	0.05739	0.09008	0.00217	100	1680.3	20.83	1686	18.91	1683.5	11.1	1743.3	40.24	0.061058

Analysis	Ratios								Concordancy	Apparent ages (Ma)								Th/U Ratio
	$^{207}Pb/^{206}Pb$	1σ	$^{206}Pb/^{238}U$	1σ	$^{207}Pb/^{235}U$	1σ	$^{208}Pb/^{232}Th$	1σ		$^{207}Pb/^{206}Pb$	1σ	$^{206}Pb/^{238}U$	1σ	$^{207}Pb/^{235}U$	1σ	$^{208}Pb/^{232}Th$	1σ	
MR14Z11C	0.10773	0.00127	0.32087	0.00413	4.76584	0.06638	0.10492	0.00275	102	1761.4	21.41	1794	20.18	1778.9	11.69	2016.6	50.35	0.095
MR14Z15C	0.10504	0.00129	0.30207	0.00386	4.37455	0.06182	0.09295	0.00266	99	1714.9	22.48	1701.6	19.09	1707.5	11.68	1796.5	49.14	0.09697
MR14Z33C	0.10865	0.00127	0.3194	0.00413	4.78417	0.06637	0.08834	0.00214	101	1776.8	21.22	1786.8	20.19	1782.1	11.65	1711	39.7	0.098084
MR14Z5C	0.10757	0.00126	0.32454	0.00417	4.81321	0.06636	0.0958	0.00232	99	1758.7	21.21	1811.9	20.31	1787.2	11.59	1849.1	42.86	0.111539
MR14Z52C	0.10756	0.00127	0.29957	0.00381	4.4434	0.0614	0.09254	0.00234	96	1758.6	21.42	1689.2	18.88	1720.5	11.45	1788.9	43.23	0.111971
MR14Z16C	0.1089	0.00136	0.30243	0.00387	4.54117	0.06491	0.09601	0.00281	96	1781.1	22.61	1703.4	19.17	1738.5	11.89	1853	51.75	0.114182
MR14Z40C	0.11093	0.00138	0.30573	0.00396	4.67532	0.06719	0.09325	0.00264	95	1814.6	22.45	1719.7	19.57	1762.8	12.02	1802	48.83	0.121228
MR14Z13C	0.10921	0.00142	0.30329	0.00402	4.56631	0.06832	0.08991	0.00282	96	1786.2	23.5	1707.6	19.87	1743.1	12.46	1740.2	52.24	0.124015
MR14Z3R	0.10653	0.00123	0.31687	0.00403	4.65379	0.06314	0.08563	0.00197	102	1740.8	21.04	1774.4	19.75	1759	11.34	1660.7	36.69	0.130822
MR14Z48C	0.10724	0.00138	0.31705	0.0041	4.68708	0.06882	0.09482	0.00314	102	1753	23.33	1775.3	20.06	1764.9	12.29	1830.9	57.91	0.131284
MR14Z6C	0.10736	0.00124	0.31901	0.0041	4.7219	0.06463	0.09562	0.00226	102	1755.1	20.85	1784.9	20.05	1771.1	11.47	1845.9	41.74	0.132286
MR14Z38C	0.108	0.00128	0.30604	0.00388	4.55683	0.06263	0.09106	0.00237	97	1765.9	21.49	1721.2	19.16	1741.4	11.44	1761.5	43.97	0.132785
MR14Z32C	0.10941	0.00125	0.32285	0.00414	4.86989	0.06632	0.09329	0.00212	101	1789.6	20.62	1803.6	20.2	1797.1	11.47	1802.7	39.15	0.137427
MR14Z30C	0.10781	0.00127	0.31627	0.00414	4.70097	0.06613	0.08705	0.00213	100	1762.8	21.24	1771.5	20.28	1767.4	11.78	1687.2	39.66	0.138225
MR14Z4C	0.10731	0.00125	0.3109	0.00406	4.59927	0.06413	0.09203	0.00222	99	1754.3	21.15	1745.1	19.95	1749.1	11.63	1779.5	41.02	0.145448
MR14Z60C	0.11131	0.00154	0.30624	0.00405	4.69843	0.07325	0.09366	0.0034	95	1820.8	24.89	1722.2	19.99	1767	13.05	1809.7	62.9	0.146187
MR14Z56C	0.10907	0.00142	0.30329	0.00398	4.55994	0.06793	0.07721	0.00233	96	1783.9	23.54	1707.6	19.71	1742	12.41	1503.3	43.63	0.153324
MR14Z46C	0.10794	0.00139	0.31579	0.0041	4.69926	0.06899	0.09416	0.00302	100	1765	23.25	1769.1	20.07	1767.1	12.29	1818.9	55.8	0.154538
MR14Z26C	0.11106	0.00125	0.31792	0.00409	4.86798	0.0659	0.09289	0.00192	98	1816.9	20.29	1779.6	20.02	1796.7	11.4	1795.3	35.57	0.15774
MR14Z55C	0.10748	0.00135	0.30712	0.004	4.55054	0.06624	0.08648	0.00249	98	1757.2	22.78	1726.5	19.7	1740.3	12.12	1676.4	46.4	0.162599
MR14Z58C	0.1102	0.00146	0.30985	0.00407	4.70713	0.07122	0.09503	0.00312	97	1802.7	23.98	1740	20.01	1768.5	12.67	1835	57.6	0.176174
MR14Z14C	0.10908	0.00135	0.30976	0.00397	4.65875	0.06621	0.09238	0.00259	98	1784.1	22.39	1739.5	19.53	1759.9	11.88	1785.9	47.91	0.176261
MR14Z39C	0.10906	0.00133	0.32088	0.00413	4.82468	0.0684	0.09546	0.00268	101	1783.8	22.05	1794	20.18	1789.2	11.92	1842.9	49.47	0.176521
MR14Z43C	0.10703	0.00144	0.29764	0.00395	4.39146	0.06735	0.0937	0.00325	96	1749.5	24.43	1679.6	19.6	1710.7	12.68	1810.4	60	0.183851
MR14Z20C	0.11042	0.0014	0.31017	0.00399	4.72215	0.06839	0.09917	0.003	96	1806.3	22.95	1741.5	19.62	1771.2	12.14	1911.1	55.15	0.188139

Analysis	Ratios								Concordancy	Apparent ages (Ma)								Th/U Ratio
	$^{207}Pb/^{206}Pb$	1σ	$^{206}Pb/^{238}U$	1σ	$^{207}Pb/^{235}U$	1σ	$^{208}Pb/^{232}Th$	1σ		$^{207}Pb/^{206}Pb$	1σ	$^{206}Pb/^{238}U$	1σ	$^{207}Pb/^{235}U$	1σ	$^{208}Pb/^{232}Th$	1σ	
MR14Z25C	0.10713	0.00123	0.3171	0.00406	4.68333	0.06347	0.08705	0.00172	101	1751.2	20.76	1775.5	19.85	1764.3	11.34	1687.1	31.99	0.235749
MR14Z21C	0.10772	0.0014	0.3172	0.00409	4.71113	0.0693	0.09423	0.00293	101	1761.2	23.5	1776.1	20.01	1769.2	12.32	1820.2	54.2	0.249879
MR14Z50C	0.10843	0.00137	0.32111	0.0042	4.80067	0.07017	0.09428	0.0025	101	1773.1	22.86	1795.1	20.51	1785	12.28	1821	46.14	0.266374
MR14Z23C	0.11083	0.00145	0.30559	0.00392	4.6697	0.06847	0.09475	0.00297	95	1813.1	23.5	1719	19.37	1761.8	12.26	1829.7	54.86	0.294178
MR14Z36C	0.10797	0.00131	0.31121	0.00399	4.63241	0.06495	0.09025	0.00208	99	1765.5	22.01	1746.6	19.64	1755.1	11.71	1746.4	38.5	0.319239
MR14Z17C	0.10791	0.00139	0.30344	0.00391	4.51473	0.06577	0.09045	0.00262	97	1764.5	23.27	1708.3	19.33	1733.7	12.11	1750.2	48.55	0.323942
MR14Z2C	0.10802	0.00126	0.30968	0.00395	4.61167	0.06285	0.09415	0.00199	98	1766.2	21.15	1739.1	19.46	1751.4	11.37	1818.6	36.76	0.341472
MR14Z28C	0.10854	0.00129	0.31509	0.00409	4.71513	0.06613	0.09094	0.00199	99	1775	21.64	1765.7	20.04	1769.9	11.75	1759.2	36.81	0.362813
MR14Z18C	0.10735	0.00139	0.30973	0.004	4.58405	0.06725	0.09113	0.00267	99	1754.8	23.46	1739.4	19.69	1746.4	12.23	1762.8	49.52	0.372325
2012MR9 Sillimanite-Biotite-Cordierite metapelitic Gneiss																		
MR9Z21R	0.0994	0.00111	0.26769	0.00322	3.66713	0.04651	0.08199	0.00194	95	1612.9	20.58	1529.1	16.35	1564.2	10.12	1592.8	36.22	0.035298
MR9Z39R	0.11266	0.00153	0.32578	0.00417	5.05845	0.07648	0.09676	0.00366	99	1842.8	24.39	1817.9	20.3	1829.2	12.82	1866.8	67.46	0.039361
MR9Z42C	0.10961	0.00139	0.30968	0.00376	4.6786	0.06542	0.09803	0.00339	97	1793	22.94	1739.1	18.52	1763.4	11.7	1890.2	62.34	0.063289
MR9Z35C	0.11015	0.00134	0.31397	0.0038	4.76641	0.06432	0.0995	0.00299	98	1801.8	21.93	1760.2	18.63	1779	11.33	1917.3	54.89	0.077346
MR9Z53C	0.19908	0.00246	0.52153	0.00693	14.29972	0.20803	0.13341	0.00404	96	2818.7	20.02	2705.7	29.36	2769.8	13.81	2531.2	72.08	0.098309
MR9Z51C	0.14095	0.00172	0.42313	0.00562	8.21506	0.11866	0.11244	0.00328	102	2238.9	20.96	2274.7	25.46	2255	13.07	2153.7	59.55	0.098601
MR9Z26C	0.10095	0.00115	0.2928	0.00357	4.07355	0.05314	0.09856	0.0024	101	1641.6	21.07	1655.5	17.8	1649	10.63	1899.9	44.24	0.102886
MR9Z23C	0.10765	0.00123	0.32191	0.00395	4.7765	0.06255	0.09013	0.00217	102	1759.9	20.72	1799.1	19.25	1780.8	11	1744.2	40.33	0.117962
MR9Z46C	0.10419	0.00118	0.29515	0.00384	4.23645	0.05795	0.08401	0.00201	98	1700.1	20.72	1667.2	19.12	1681.1	11.24	1630.4	37.54	0.138308
MR9Z38R	0.13243	0.00176	0.38267	0.00485	6.98493	0.10376	0.10729	0.00392	98	2130.4	23.14	2088.7	22.62	2109.5	13.19	2059.9	71.47	0.141201
MR9ZR1C	0.15808	0.00185	0.42305	0.00527	9.21854	0.12266	0.12291	0.00284	102	2435.2	19.71	2274.3	23.86	2360	12.19	2343	51.12	0.159069
MR9Z52C	0.14401	0.00177	0.42892	0.00567	8.50632	0.12301	0.11088	0.00326	101	2275.9	21.07	2300.9	25.58	2286.6	13.14	2125.4	59.37	0.17898
MR9ZR12C	0.11139	0.00148	0.31869	0.00406	4.89313	0.07236	0.08858	0.00296	98	1822.1	23.88	1783.3	19.86	1801.1	12.47	1715.4	55.04	0.179964
MR9ZR5C	0.18142	0.00203	0.49659	0.00603	12.41912	0.15877	0.1369	0.003	97	2665.9	18.41	2599.1	25.96	2636.6	12.01	2593.3	53.37	0.188915
MR9ZR14C	0.10758	0.00132	0.31049	0.00377	4.6041	0.0624	0.09815	0.0028	99	1758.8	22.16	1743.1	18.54	1750	11.31	1892.5	51.6	0.195988

Analysis	Ratios								Concordancy	Apparent ages (Ma)								Th/U Ratio
	$^{207}Pb/^{206}Pb$	1σ	$^{206}Pb/^{238}U$	1σ	$^{207}Pb/^{235}U$	1σ	$^{208}Pb/^{232}Th$	1σ		$^{207}Pb/^{206}Pb$	1σ	$^{206}Pb/^{238}U$	1σ	$^{207}Pb/^{235}U$	1σ	$^{208}Pb/^{232}Th$	1σ	
MR9ZR10C	0.11681	0.00137	0.34786	0.00422	5.60119	0.07373	0.10153	0.00246	101	1907.9	20.9	1924.4	20.2	1916.3	11.34	1954.6	45.17	0.198059
MR9Z47C	0.10578	0.00125	0.30027	0.004	4.3767	0.06222	0.08221	0.00214	98	1728	21.54	1692.7	19.81	1708	11.75	1596.8	39.97	0.209003
MR9Z54C	0.11279	0.00159	0.339	0.00469	5.2668	0.08497	0.08365	0.00308	102	1844.8	25.33	1881.9	22.56	1863.5	13.77	1623.7	57.4	0.215658
MR9ZR20C	0.1634	0.00223	0.44541	0.00567	10.0301	0.15086	0.12346	0.00468	95	2491.1	22.78	2374.8	25.28	2437.6	13.89	2352.9	84.28	0.234595
MR9Z29C	0.11337	0.00136	0.3285	0.00406	5.13285	0.06978	0.09611	0.00259	99	1854.1	21.58	1831.1	19.72	1841.6	11.55	1854.8	47.83	0.259103
MR9Z43R	0.11512	0.0013	0.3273	0.00422	5.19136	0.07001	0.09011	0.00195	97	1881.7	20.18	1825.3	20.5	1851.2	11.48	1744	36.22	0.261035
MR9Z30C	0.11046	0.00133	0.3256	0.00392	4.95694	0.06619	0.09991	0.00279	101	1807	21.76	1817	19.04	1812	11.28	1924.8	51.32	0.263862
MR9Z41C	0.13143	0.00171	0.38736	0.00483	7.01731	0.10171	0.11136	0.00384	100	2117.2	22.67	2110.6	22.46	2113.6	12.88	2134.1	69.83	0.267086
MR9ZR11C	0.11625	0.00142	0.32384	0.00395	5.1892	0.07036	0.10161	0.00273	95	1899.4	21.81	1808.4	19.25	1850.8	11.54	1955.9	50.18	0.271807
MR9Z33C	0.11697	0.0014	0.32421	0.00391	5.22651	0.06977	0.09859	0.0028	95	1910.4	21.38	1810.3	19.03	1856.9	11.38	1900.5	51.47	0.281767
MR9ZR13C	0.14823	0.00198	0.41202	0.00524	8.41764	0.12396	0.12293	0.00406	96	2325.6	22.74	2224.2	23.93	2277.1	13.37	2343.5	73.07	0.293382
MR9Z27C	0.11379	0.00135	0.32244	0.00399	5.05671	0.06833	0.09578	0.0025	97	1860.8	21.33	1801.7	19.47	1828.9	11.45	1848.7	46.06	0.297011
MR9Z48C	0.11773	0.00137	0.32707	0.00427	5.30409	0.07357	0.09392	0.00231	95	1922.1	20.67	1824.2	20.75	1869.5	11.85	1814.5	42.63	0.321417
MR9Z32C	0.10852	0.00166	0.30908	0.00412	4.62416	0.07627	0.08076	0.00285	98	1774.7	27.69	1736.2	20.31	1753.6	13.77	1569.7	53.37	0.379287
MR9Z31C	0.11072	0.00146	0.33036	0.00413	5.04117	0.07285	0.09467	0.0028	102	1811.2	23.82	1840.1	19.99	1826.3	12.24	1828.3	51.72	0.398941
MR9ZR18C	0.10951	0.00159	0.32522	0.00423	4.90932	0.07815	0.08967	0.00359	101	1791.2	26.29	1815.2	20.58	1803.9	13.43	1735.8	66.6	0.401533
MR9ZR16C	0.1388	0.00177	0.4164	0.00517	7.96664	0.11282	0.11718	0.00381	101	2212.3	21.94	2244.1	23.55	2227.3	12.78	2239.6	68.93	0.407333
MR9ZR19C	0.10601	0.00142	0.31563	0.00397	4.6121	0.06799	0.09414	0.00325	102	1732	24.45	1768.3	19.46	1751.5	12.3	1818.5	59.96	0.409456
MR9Z25C	0.11192	0.00129	0.33113	0.00404	5.10748	0.06689	0.09486	0.00229	101	1830.7	20.72	1843.8	19.58	1837.3	11.12	1831.7	42.27	0.415252
MR9ZR17C	0.10656	0.00152	0.29378	0.00378	4.31512	0.06736	0.08906	0.00333	95	1741.5	25.84	1660.4	18.86	1696.3	12.87	1724.4	61.77	0.424132
MR9ZR3C	0.16325	0.00207	0.45979	0.0059	10.34667	0.14748	0.12453	0.00327	98	2489.6	21.25	2438.6	26.06	2466.3	13.2	2372.1	58.7	0.429994
MR9ZR9C	0.16253	0.00194	0.45435	0.00567	10.17867	0.13854	0.1268	0.0033	97	2482.1	19.98	2414.6	25.13	2451.1	12.58	2413	59.11	0.433997
MR9Z22C	0.13119	0.00148	0.36499	0.00438	6.59922	0.08413	0.10658	0.00235	95	2114	19.67	2005.8	20.7	2059.2	11.24	2047	43.01	0.436531
MR9Z37C	0.13519	0.00169	0.39027	0.00475	7.27202	0.10029	0.113	0.00347	98	2166.5	21.66	2124.1	22.04	2145.4	12.31	2164	62.94	0.57777
MR9ZR2C	0.10528	0.00122	0.30278	0.00367	4.39454	0.05734	0.0867	0.00181	99	1719.3	21.12	1705.1	18.18	1711.3	10.79	1680.5	33.58	0.597511

Analysis	Ratios								Concordancy	Apparent ages (Ma)								Th/U Ratio
	$^{207}Pb/^{206}Pb$	1σ	$^{206}Pb/^{238}U$	1σ	$^{207}Pb/^{235}U$	1σ	$^{208}Pb/^{232}Th$	1σ		$^{207}Pb/^{206}Pb$	1σ	$^{206}Pb/^{238}U$	1σ	$^{207}Pb/^{235}U$	1σ	$^{208}Pb/^{232}Th$	1σ	
MR9Z28C	0.11044	0.00146	0.31701	0.00402	4.82527	0.07007	0.09285	0.00251	98	1806.7	23.79	1775.1	19.67	1789.3	12.21	1794.6	46.38	0.609556
MR9Z44C	0.14033	0.00164	0.4171	0.00558	8.06595	0.11353	0.09921	0.00228	101	2231.3	20.09	2247.3	25.38	2238.4	12.72	1912	41.87	0.66497
MR9ZR7C	0.16549	0.002	0.47782	0.00594	10.90008	0.14714	0.13224	0.00306	100	2512.5	20.16	2517.8	25.92	2514.6	12.55	2510.2	54.7	0.707519
MR9Z40C	0.10766	0.00139	0.31475	0.00385	4.67042	0.06597	0.09296	0.00304	100	1760.1	23.32	1764.1	18.86	1762	11.81	1796.6	56.3	0.774502

NAP-11a Sillimanite-Biotite-Cordierite metapelitic Gneiss

Analysis	Ratios								Concordancy	Apparent ages (Ma)								Th/U Ratio
NAP11A_Z55_1R	0.101	0.00146	0.28972	0.0045	4.03361	0.07183	0.12771	0.00738	100	1642.6	26.65	1640.2	22.47	1641	14.49	2429.4	132.19	0.004123
NAP11A_Z61_1R	0.09958	0.00125	0.28652	0.00434	3.9336	0.06416	0.14579	0.0067	100	1616.3	23.26	1624.1	21.74	1620.6	13.2	2750.7	118.21	0.005156
NAP11A_Z37_1R	0.10151	0.00118	0.30174	0.00453	4.22264	0.06616	0.15673	0.00534	103	1651.9	21.46	1699.9	22.44	1678.4	12.86	2942.9	93.36	0.005318
NAP11A_Z59_2R	0.10114	0.00121	0.28419	0.00427	3.96267	0.06279	0.13083	0.00497	98	1645.1	22.04	1612.4	21.43	1626.6	12.85	2485.1	88.86	0.005377
NAP11A_Z34_1R	0.0996	0.00127	0.2847	0.00428	3.909	0.06396	0.15017	0.00638	100	1616.7	23.5	1615	21.5	1615.5	13.23	2827.9	112.09	0.006317
NAP11A_Z51_1R	0.10463	0.00141	0.30206	0.0047	4.35628	0.0751	0.11052	0.00464	100	1707.8	24.53	1701.5	23.26	1704.1	14.24	2118.8	84.38	0.008721
NAP11A_Z22_1R	0.10597	0.00134	0.31129	0.00464	4.54804	0.07375	0.12281	0.00464	101	1731.3	22.95	1747.1	22.8	1739.8	13.5	2341.3	83.52	0.009813
NAP11A_Z29_1R	0.11522	0.00134	0.32032	0.0047	5.08733	0.07809	0.10596	0.00339	95	1883.3	20.83	1791.3	22.96	1834	13.03	2035.6	61.87	0.009907
NAP11A_Z53_1R	0.1241	0.00182	0.36396	0.00577	6.22627	0.11364	0.11724	0.00547	99	2016	25.77	2000.9	27.29	2008.1	15.97	2240.8	98.96	0.016996
NAP11A_Z03_2R	0.10408	0.00124	0.28403	0.00409	4.07533	0.0623	0.10298	0.00328	97	1698.2	21.72	1611.6	20.51	1649.4	12.46	1981.1	60.05	0.01803
NAP11A_Z18_2R	0.11178	0.00131	0.33369	0.00495	5.1426	0.0805	0.10103	0.00286	102	1828.6	21.09	1856.2	23.93	1843.2	13.31	1945.3	52.59	0.025624
NAP11A_Z25_1C	0.11515	0.00149	0.3429	0.00509	5.44362	0.08926	0.10369	0.0036	101	1882.2	23.11	1900.6	24.45	1891.8	14.07	1994	65.91	0.026219
NAP11A_Z47_1R	0.12182	0.0017	0.35691	0.00574	5.99309	0.10792	0.10486	0.00438	99	1983.1	24.68	1967.5	27.28	1974.8	15.67	2015.5	80.14	0.027733
NAP11A_Z09_2R	0.11404	0.00147	0.32767	0.00482	5.15194	0.08365	0.09532	0.00319	98	1864.8	23.03	1827.1	23.39	1844.7	13.81	1840.2	58.9	0.035045
NAP11A_Z38_1R	0.11736	0.00147	0.36042	0.00574	5.83064	0.09894	0.09501	0.00301	104	1916.4	22.27	1984.2	27.18	1951	14.71	1834.5	55.54	0.037527
NAP11A_Z64_1R	0.15481	0.002	0.42671	0.00649	9.10765	0.15128	0.12249	0.00433	95	2399.8	21.76	2290.9	29.32	2348.9	15.2	2335.4	77.93	0.045601
NAP11A_Z62_1R	0.13546	0.00168	0.39902	0.00603	7.45208	0.12097	0.10869	0.00351	100	2170	21.46	2164.5	27.78	2167.2	14.53	2085.6	64.03	0.054945
NAP11A_Z17_1R	0.11054	0.00153	0.31037	0.00468	4.72971	0.08099	0.12706	0.0052	96	1808.3	24.86	1742.5	23.05	1772.5	14.35	2417.7	93.22	0.068036
NAP11A_Z06_1R	0.12474	0.00151	0.35472	0.00515	6.09961	0.09521	0.11521	0.00353	97	2025	21.32	1957.1	24.51	1990.2	13.62	2204	64.06	0.079338
NAP11A_Z30_1R	0.11748	0.00141	0.33777	0.00499	5.46972	0.08549	0.10342	0.003	98	1918.2	21.35	1876	24.07	1895.9	13.42	1989.2	55.01	0.082376

Analysis	Ratios								Concordancy	Apparent ages (Ma)								Th/U Ratio
	$^{207}Pb/^{206}Pb$	1σ	$^{206}Pb/^{238}U$	1σ	$^{207}Pb/^{235}U$	1σ	$^{208}Pb/^{232}Th$	1σ		$^{207}Pb/^{206}Pb$	1σ	$^{206}Pb/^{238}U$	1σ	$^{207}Pb/^{235}U$	1σ	$^{208}Pb/^{232}Th$	1σ	
NAP11A_Z04_1R	0.10987	0.00131	0.30762	0.00444	4.65918	0.07156	0.12291	0.00352	96	1797.2	21.52	1729	21.87	1759.9	12.84	2343.1	63.4	0.084923
NAP11A_Z12_1C	0.11947	0.00148	0.35866	0.00535	5.90739	0.09523	0.10806	0.00352	97	1948.4	21.91	1975.8	25.38	1962.3	14	2074	64.24	0.105119
NAP11A_Z42_1R	0.12622	0.00168	0.359	0.00572	6.24623	0.10929	0.1254	0.00456	97	2045.9	23.36	1977.4	27.15	2010.9	15.31	2387.9	81.86	0.105411
NAP11A_Z19_1R	0.12644	0.00154	0.35647	0.00525	6.21413	0.09806	0.13417	0.00402	96	2049.1	21.35	1965.4	24.95	2006.4	13.8	2544.7	71.63	0.113472
NAP11A_Z10_1R	0.12004	0.00146	0.33381	0.00498	5.52418	0.08838	0.11891	0.00356	95	1956.8	21.54	1856.8	24.07	1904.4	13.75	2271	64.24	0.126933
NAP11A_Z14_1R	0.17005	0.00216	0.48385	0.00723	11.3435	0.18559	0.14832	0.00522	99	2558.2	21.11	2544	31.43	2551.8	15.27	2795.3	91.82	0.129791
NAP11A_Z45_1R	0.11378	0.00151	0.34488	0.00532	5.40986	0.09202	0.09938	0.00364	103	1860.6	23.76	1910.1	25.5	1886.4	14.58	1915.1	66.99	0.138702
NAP11A_Z36_1C	0.11787	0.0015	0.35866	0.00542	5.82812	0.09599	0.10711	0.00367	103	1924.2	22.57	1975.8	25.74	1950.6	14.27	2056.7	66.98	0.142168
NAP11A_Z56_1R	0.1474	0.00282	0.41643	0.00699	8.46066	0.18455	0.13802	0.00866	97	2316	32.49	2244.3	31.83	2281.7	19.81	2613.2	153.77	0.146311
NAP11A_Z26_1R	0.11775	0.00157	0.35579	0.0053	5.77562	0.09619	0.11533	0.00413	102	1922.3	23.69	1962.2	25.2	1942.8	14.42	2206.2	74.83	0.179846
NAP11A_Z05_1C	0.11265	0.00136	0.3277	0.00475	5.08889	0.07904	0.096	0.00282	99	1842.5	21.73	1827.2	23.04	1834.3	13.18	1852.8	51.99	0.222834
NAP11A_Z43_1R	0.13326	0.00167	0.40168	0.00607	7.37964	0.12013	0.11336	0.00365	102	2141.4	21.74	2176.8	27.89	2158.5	14.56	2170.5	66.2	0.237246
NAP11A_Z63_1R	0.11517	0.00148	0.34624	0.00527	5.49749	0.09117	0.09692	0.00324	102	1882.5	23.02	1916.6	25.23	1900.2	14.25	1869.8	59.64	0.246803
NAP11A_Z27_1C	0.13157	0.00153	0.37507	0.00548	6.80252	0.10344	0.10803	0.00276	97	2119.1	20.18	2053.2	25.69	2086.1	13.46	2073.4	50.27	0.255015
NAP11A_Z02_1C	0.10921	0.00141	0.30154	0.00439	4.53968	0.07239	0.09655	0.00263	95	1786.3	23.45	1698.9	21.74	1738.3	13.27	1862.9	48.54	0.256143
NAP11A_Z60_1R	0.11465	0.00137	0.34001	0.00511	5.37477	0.08519	0.09738	0.00278	101	1874.5	21.38	1886.7	24.57	1880.8	13.57	1878.2	51.14	0.257108
NAP11A_Z58_1C	0.11254	0.00131	0.33449	0.00501	5.19007	0.08102	0.09561	0.0025	101	1840.8	20.99	1860.1	24.19	1851	13.29	1845.6	46.16	0.257971
NAP11A_Z24_1C	0.15101	0.002	0.43879	0.00658	9.13545	0.15165	0.12426	0.00422	99	2357.4	22.42	2345.2	29.47	2351.7	15.19	2367.4	75.92	0.261265
NAP11A_Z11_1R	0.11139	0.00134	0.3396	0.00505	5.21496	0.083	0.10838	0.00327	103	1822.2	21.7	1884.8	24.32	1855.1	13.56	2079.8	59.54	0.280777
NAP11A_Z16_1C	0.13432	0.00182	0.38972	0.00588	7.21703	0.12212	0.12846	0.00493	98	2155.3	23.41	2121.5	27.26	2138.6	15.09	2442.7	88.29	0.304594
NAP11A_Z46_1C	0.13938	0.0019	0.41113	0.00607	7.89924	0.13198	0.1253	0.00495	100	2219.5	23.43	2220.1	27.74	2219.6	15.06	2386	88.84	0.326444
NAP11A_Z35_1C	0.12556	0.00182	0.35718	0.00554	6.18228	0.10895	0.10164	0.00354	97	2036.7	25.42	1968.8	26.3	2001.9	15.4	1956.5	64.86	0.345651
NAP11A_Z11_1C	0.1112	0.00138	0.32646	0.00488	5.00458	0.08085	0.09588	0.00301	100	1819.1	22.36	1821.2	23.7	1820.1	13.67	1850.6	55.45	0.346694
NAP11A_Z08_1C	0.1142	0.00144	0.32919	0.00482	5.18275	0.08294	0.0945	0.00306	98	1867.3	22.54	1834.4	23.35	1849.8	13.62	1825	56.49	0.347744
NAP11A_Z44_1R	0.14585	0.00227	0.42521	0.00704	8.54883	0.16312	0.1122	0.00461	99	2297.8	26.45	2284.1	31.84	2291.1	17.35	2149.4	83.87	0.359885

Analysis	Ratios								Concordancy	Apparent ages (Ma)								Th/U Ratio
	$^{207}Pb/^{206}Pb$	1σ	$^{206}Pb/^{238}U$	1σ	$^{207}Pb/^{235}U$	1σ	$^{208}Pb/^{232}Th$	1σ		$^{207}Pb/^{206}Pb$	1σ	$^{206}Pb/^{238}U$	1σ	$^{207}Pb/^{235}U$	1σ	$^{208}Pb/^{232}Th$	1σ	
NAP11A_Z31_1C	0.11046	0.00133	0.33386	0.00495	5.08342	0.07983	0.09389	0.0027	103	1807	21.67	1857.1	23.91	1833.3	13.32	1813.9	49.89	0.37773
NAP11A_Z39_1C	0.12773	0.00168	0.38004	0.0058	6.69138	0.11236	0.11417	0.00395	100	2066.9	23.06	2076.4	27.08	2071.5	14.83	2185.2	71.65	0.385477
NAP11A_Z54_1OC	0.16023	0.00213	0.45635	0.00684	10.07957	0.16708	0.13692	0.0049	99	2458.1	22.28	2423.4	30.27	2442.1	15.31	2593.7	87.07	0.391141
NAP11A_Z21_1C	0.14932	0.00183	0.43504	0.00647	8.95611	0.14316	0.125	0.00378	100	2338.2	20.86	2328.4	29.06	2333.5	14.6	2380.6	67.84	0.398178
NAP11A_Z01_1IC	0.14889	0.00181	0.42112	0.00608	8.64314	0.1326	0.12196	0.00312	101	2333.1	20.68	2265.6	27.6	2301.1	13.96	2326	56.17	0.399611
NAP11A_Z41_1C	0.14295	0.00191	0.40222	0.00628	7.92666	0.13586	0.12896	0.00441	96	2263.2	22.89	2179.3	28.85	2222.7	15.45	2451.7	78.96	0.402229
NAP11A_Z61_2C	0.16337	0.00214	0.47057	0.00721	10.59921	0.17631	0.1282	0.00402	100	2490.9	21.88	2486	31.6	2488.6	15.43	2438.1	72.01	0.458743
NAP11A_Z09_1C	0.11404	0.00147	0.32767	0.00482	5.15194	0.08365	0.09532	0.00319	98	1864.8	23.03	1827.1	23.39	1844.7	13.81	1840.2	58.9	0.469057
NAP11A_Z50_1C	0.1455	0.00235	0.41633	0.0069	8.34941	0.16326	0.11548	0.00513	98	2293.7	27.53	2243.8	31.42	2269.7	17.73	2208.9	92.92	0.470472
NAP11A_Z49_1R	0.15495	0.00259	0.45095	0.00758	9.63111	0.19399	0.1198	0.00588	100	2401.3	28.1	2399.5	33.67	2400.1	18.53	2287	106.22	0.506344

APPENDIX A: U-PB LA-ICPMS MONAZITE DATA

Analysis	Ratios						Concordancy	Apparent ages (Ma)					
	$^{207}Pb/^{206}Pb$	1σ	$^{206}Pb/^{238}U$	1σ	$^{207}Pb/^{235}U$	1σ		$^{207}Pb/^{206}Pb$	1σ	$^{206}Pb/^{238}U$	1σ	$^{207}Pb/^{235}U$	1σ
NAP4- Napperby gneiss with planar S₃ fabric													
NAP4M2A	0.09587	0.00114	0.25447	0.00432	3.36278	0.05926	102	1545.1	22.09	1461.5	22.22	1495.8	13.79
NAP4M10A	0.09944	0.0012	0.28754	0.005	3.94221	0.07111	100	1613.7	22.28	1629.2	25.02	1622.4	14.61
NAP4M12A	0.10237	0.00114	0.29865	0.00515	4.21444	0.07365	100	1667.6	20.54	1684.6	25.57	1676.8	14.34
NAP4M14A	0.10276	0.00118	0.28704	0.00496	4.06546	0.0719	101	1674.5	21.08	1626.7	24.87	1647.4	14.41
NAP4M4A	0.10364	0.00108	0.29465	0.00501	4.20893	0.07124	101	1690.2	19.18	1664.7	24.92	1675.8	13.89
NAP4M8A	0.10536	0.00112	0.2932	0.005	4.25727	0.0727	102	1720.5	19.36	1657.5	24.93	1685.1	14.04
NAP4M9B	0.10555	0.00114	0.29145	0.00498	4.24042	0.07279	102	1723.9	19.72	1648.8	24.85	1681.9	14.1
NAP4M5A	0.10584	0.0011	0.30488	0.00518	4.44705	0.07519	100	1728.9	18.97	1715.5	25.6	1721.1	14.02
NAP4M15A	0.10619	0.00121	0.31054	0.00538	4.54513	0.08024	100	1735	20.74	1743.4	26.45	1739.3	14.69
NAP4M6A	0.10738	0.00112	0.308	0.00524	4.55782	0.07709	101	1755.5	18.85	1730.8	25.81	1741.6	14.08
NAP4M7A	0.10826	0.00114	0.31179	0.00531	4.65231	0.07903	101	1770.3	19.11	1749.5	26.1	1758.7	14.2
NAP4M13A	0.10851	0.00138	0.32253	0.00559	4.81969	0.08936	99	1774.4	23.12	1802.1	27.26	1788.3	15.59
NAP13- Leucosome with retrogressed garnet													
NAP13M18	0.09552	0.00101	0.27101	0.00474	3.56717	0.06214	100	1538.4	19.73	1545.9	24.05	1542.3	13.81
NAP13M1A	0.09563	0.00097	0.26316	0.00453	3.46791	0.05912	98	1540.5	18.95	1506	23.13	1519.9	13.44
NAP13M9A	0.09584	0.00098	0.27906	0.00483	3.68557	0.06318	103	1544.6	19.09	1586.6	24.36	1568.2	13.69
NAP13M14	0.09593	0.001	0.26627	0.00464	3.51994	0.06103	98	1546.5	19.53	1521.8	23.65	1531.7	13.71
NAP13M16	0.09598	0.00101	0.26951	0.00471	3.56446	0.06191	99	1547.4	19.58	1538.3	23.9	1541.7	13.77
NAP13M2A	0.09611	0.00097	0.26494	0.00457	3.50907	0.05981	98	1550	18.89	1515.1	23.27	1529.3	13.47
NAP13M12	0.09612	0.00101	0.2797	0.00487	3.70474	0.06421	103	1550.1	19.54	1589.9	24.55	1572.4	13.86
NAP13M17	0.09612	0.00102	0.26656	0.00466	3.53065	0.06149	98	1550.1	19.72	1523.3	23.72	1534.1	13.78

NAP13M15	0.09621	0.00101	0.26451	0.00462	3.50675	0.06087	97	1551.9	19.56	1512.9	23.54	1528.7	13.71
NAP13M8A	0.09653	0.00098	0.27369	0.00474	3.6406	0.06234	100	1558	19.01	1559.5	23.97	1558.5	13.64
NAP13M20	0.09652	0.00103	0.27231	0.00477	3.62193	0.06333	100	1558	19.86	1552.5	24.18	1554.4	13.91
NAP13M5A	0.09665	0.00098	0.27438	0.00474	3.65443	0.06244	100	1560.4	18.94	1563	23.97	1561.5	13.62
NAP13M3A	0.0967	0.00098	0.27997	0.00483	3.73054	0.06363	102	1561.3	18.88	1591.2	24.32	1577.9	13.66
NAP13M7A	0.0968	0.00099	0.27001	0.00467	3.60166	0.06163	99	1563.3	18.98	1540.8	23.7	1549.9	13.6
NAP13M13	0.09691	0.00101	0.26964	0.0047	3.60085	0.06234	98	1565.5	19.41	1539	23.86	1549.7	13.76
NAP13M4A	0.097	0.00098	0.28157	0.00486	3.76355	0.06424	102	1567.1	18.89	1599.3	24.44	1585	13.69
NAP13M6A	0.09744	0.00099	0.27149	0.00469	3.64537	0.0623	98	1575.6	18.9	1548.3	23.78	1559.5	13.62
2012MR6- Garnet absent leucratic melt													
M9	0.09439	0.00098	0.25814	0.00333	3.35984	0.04385	97.65156013	1515.9	19.42	1480.3	17.05	1495.1	10.21
M4	0.09446	0.00097	0.26674	0.00341	3.47424	0.04477	100.4547552	1517.3	19.26	1524.2	17.35	1521.4	10.16
M15	0.09555	0.00102	0.27261	0.00359	3.59139	0.04855	100.9812204	1538.9	19.94	1554	18.16	1547.6	10.74
M12	0.09559	0.00101	0.27157	0.00356	3.57927	0.04807	100.5975578	1539.6	19.75	1548.8	18.07	1544.9	10.66
M13	0.09588	0.00101	0.26177	0.00343	3.46059	0.04623	96.99107027	1545.4	19.61	1498.9	17.53	1518.3	10.52
M7	0.09614	0.00099	0.26298	0.00338	3.48638	0.04517	97.07191229	1550.5	19.19	1505.1	17.24	1524.1	10.22
M16	0.09621	0.00102	0.27257	0.0036	3.61583	0.04898	100.1353267	1551.8	19.84	1553.9	18.23	1553	10.78
M1	0.09647	0.00099	0.263	0.00335	3.49892	0.0449	96.66666667	1557	19.16	1505.1	17.08	1527	10.13
M10	0.09663	0.001	0.26006	0.00336	3.46527	0.04525	95.51951798	1560.1	19.26	1490.2	17.18	1519.3	10.29
M3	0.09677	0.00099	0.26467	0.00338	3.53193	0.04546	96.85820322	1562.8	19.13	1513.7	17.21	1534.4	10.18
M5	0.09757	0.001	0.27427	0.00351	3.69027	0.04765	98.99258696	1578.3	19.1	1562.4	17.76	1569.3	10.31
M8	0.09807	0.00102	0.26664	0.00343	3.60569	0.04697	95.96296763	1587.8	19.37	1523.7	17.44	1550.8	10.36
M19	0.10054	0.0011	0.28894	0.00384	4.00518	0.05545	100.1285111	1634.1	20.24	1636.2	19.18	1635.2	11.25
2012MR9- Siilimanite-codierite-biotite metapelite													
M8	0.09531	0.00102	0.27102	0.00393	3.56118	0.05228	100	1534.1	19.93	1546	19.91	1540.9	11.64
M5	0.09554	0.00099	0.26916	0.00393	3.54582	0.05191	103	1538.8	19.41	1536.5	19.96	1537.5	11.59
M7	0.09566	0.001	0.27121	0.00395	3.57723	0.05237	102	1541.2	19.58	1546.9	20.02	1544.5	11.62
M24	0.09582	0.00106	0.26808	0.00386	3.54165	0.05247	95	1544.3	20.57	1531	19.63	1536.6	11.73

M20	0.09604	0.00105	0.26722	0.00385	3.5382	0.05236	96	1548.5	20.39	1526.7	19.61	1535.8	11.72
M12	0.09621	0.00102	0.27136	0.00394	3.59962	0.05276	101	1551.9	19.7	1547.7	19.97	1549.4	11.65
M2	0.09624	0.001	0.26341	0.00384	3.49517	0.05111	101	1552.4	19.38	1507.3	19.6	1526.1	11.55
M16	0.09628	0.00105	0.26632	0.00385	3.53505	0.05222	97	1553.1	20.25	1522.1	19.59	1535.1	11.69
M6	0.0964	0.00101	0.27072	0.00394	3.59821	0.05272	103	1555.6	19.5	1544.4	20.01	1549.1	11.64
M4	0.09642	0.001	0.26615	0.00389	3.53845	0.05176	102	1556	19.31	1521.3	19.79	1535.9	11.58
M19	0.09653	0.00106	0.26659	0.00384	3.54794	0.05248	96	1558.1	20.41	1523.4	19.56	1538	11.72
M22	0.09655	0.00107	0.26932	0.00388	3.58525	0.05331	96	1558.6	20.61	1537.4	19.72	1546.3	11.8
M21	0.09664	0.00106	0.26688	0.00385	3.55581	0.05255	96	1560.2	20.34	1524.9	19.59	1539.7	11.71
M10R	0.09666	0.00102	0.27005	0.00393	3.59909	0.0529	101	1560.7	19.74	1541	19.93	1549.3	11.68
M17	0.0967	0.00106	0.26676	0.00384	3.55641	0.05257	95	1561.3	20.48	1524.3	19.52	1539.9	11.71
M18	0.0967	0.00105	0.26397	0.00381	3.51926	0.05196	96	1561.4	20.24	1510.1	19.44	1531.6	11.67
M11	0.09672	0.00102	0.27028	0.00392	3.60441	0.05274	102	1561.9	19.59	1542.2	19.91	1550.5	11.63
M13	0.09676	0.00105	0.27394	0.00394	3.65445	0.05369	99	1562.5	20.16	1560.8	19.94	1561.5	11.71
M3	0.09676	0.001	0.26124	0.00381	3.48537	0.05085	101	1562.6	19.3	1496.2	19.45	1523.9	11.51
M14	0.09679	0.00105	0.27493	0.00395	3.66881	0.05392	99	1563.1	20.25	1565.8	19.98	1564.6	11.73
M15	0.09679	0.00105	0.26549	0.00382	3.54298	0.05212	96	1563.1	20.27	1517.9	19.47	1536.9	11.65
M1	0.09704	0.001	0.27155	0.00396	3.63316	0.05305	104	1568	19.26	1548.7	20.08	1556.8	11.63
M23	0.09712	0.00108	0.26941	0.00388	3.60757	0.05366	95	1569.6	20.68	1537.8	19.71	1551.2	11.83

2012MR11- Sillimanite-cordierite biotite metapelitic gneiss from the hinge of F4 fold

M10	0.09541	0.001	0.27138	0.00351	3.56978	0.04697	100	1536.2	19.67	1547.8	17.8	1542.8	10.44
M7	0.09563	0.00101	0.27353	0.00354	3.60655	0.04746	100	1540.6	19.68	1558.7	17.9	1551	10.46
M1	0.09577	0.00099	0.27219	0.00353	3.59359	0.04678	100	1543.3	19.31	1551.9	17.87	1548.1	10.34
M11	0.09584	0.00103	0.28103	0.00362	3.71332	0.04923	99	1544.6	20.07	1596.6	18.21	1574.2	10.61
M6	0.0959	0.00101	0.27004	0.00347	3.57055	0.04676	100	1545.8	19.73	1541	17.59	1543	10.39
M3	0.096	0.001	0.26929	0.00349	3.56312	0.04633	100	1547.9	19.39	1537.2	17.72	1541.4	10.31
M14	0.0961	0.00104	0.26643	0.00345	3.52964	0.04715	101	1549.7	20.22	1522.7	17.54	1533.9	10.57
M12	0.09612	0.00103	0.2762	0.00357	3.65988	0.04854	99	1550.1	19.97	1572.2	18.03	1562.7	10.58

M16	0.09622	0.00105	0.2698	0.00349	3.57904	0.04787	100	1552.2	20.27	1539.8	17.71	1544.9	10.61
M5	0.09643	0.00101	0.26875	0.00347	3.57291	0.04676	101	1556.1	19.47	1534.4	17.65	1543.5	10.38
M18	0.09643	0.00109	0.26725	0.00344	3.55288	0.04832	101	1556.2	21.05	1526.8	17.48	1539.1	10.78
M2	0.09644	0.00099	0.26176	0.00339	3.47886	0.04492	102	1556.3	19.18	1498.8	17.3	1522.4	10.18
M13	0.09664	0.00105	0.2752	0.00356	3.66619	0.04913	100	1560.3	20.33	1567.1	18.02	1564	10.69
M17	0.09678	0.00107	0.2786	0.00359	3.71741	0.04993	99	1563	20.52	1584.3	18.08	1575.1	10.75
M4	0.09683	0.00101	0.27945	0.00362	3.72985	0.04879	99	1564	19.46	1588.6	18.26	1577.8	10.47
M15	0.09688	0.00105	0.28252	0.00365	3.77303	0.05025	99	1565	20.13	1604	18.36	1587	10.69
M20	0.09728	0.00109	0.26848	0.00347	3.6005	0.04889	101	1572.6	20.8	1533.1	17.63	1549.6	10.79
M19	0.09744	0.0011	0.2832	0.00362	3.80412	0.05154	99	1575.7	21.02	1607.5	18.2	1593.6	10.89
M9	0.09751	0.00103	0.27733	0.00359	3.72781	0.04906	100	1577.1	19.69	1577.9	18.11	1577.4	10.54
M8	0.0985	0.00105	0.27568	0.00357	3.74392	0.04957	101	1596	19.78	1569.6	18.03	1580.8	10.61

2012MR14- Granitic Gneiss with two fabrics

M3	0.0954	0.00097	0.26361	0.00339	3.46725	0.04463	101	1536	19.09	1508.3	17.31	1519.8	10.14
M15	0.09555	0.00102	0.2663	0.00343	3.50805	0.04638	100	1539	19.94	1522	17.48	1529	10.45
M7	0.09621	0.00099	0.25589	0.00329	3.39427	0.04397	102	1551.9	19.28	1468.8	16.9	1503.1	10.16
M1	0.09675	0.00099	0.26767	0.00345	3.57023	0.0461	101	1562.3	19.09	1528.9	17.55	1542.9	10.24
M8	0.09681	0.001	0.25977	0.00334	3.46727	0.04497	102	1563.6	19.28	1488.7	17.11	1519.8	10.22
M4	0.09687	0.00099	0.26206	0.00337	3.50003	0.04514	102	1564.7	19.11	1500.4	17.21	1527.2	10.19
M5	0.09688	0.00099	0.2573	0.00331	3.43672	0.0443	102	1565	19.1	1476	16.95	1512.8	10.14
M18	0.0969	0.00104	0.26231	0.00337	3.5045	0.04641	102	1565.3	20.02	1501.6	17.22	1528.2	10.46
M13	0.09704	0.00104	0.27378	0.00353	3.6624	0.0485	100	1567.9	19.98	1560	17.87	1563.2	10.56
M10	0.09711	0.001	0.25785	0.00331	3.45215	0.04462	103	1569.4	19.21	1478.8	16.96	1516.4	10.18
M9	0.09713	0.001	0.25713	0.0033	3.44301	0.04456	103	1569.7	19.24	1475.1	16.94	1514.3	10.18
M14	0.09715	0.00103	0.26384	0.0034	3.53381	0.04656	102	1570.2	19.76	1509.5	17.34	1534.8	10.43
M2	0.09722	0.00099	0.25985	0.00334	3.48264	0.0448	102	1571.4	19.04	1489.1	17.08	1523.3	10.15
M19	0.09728	0.00106	0.26491	0.00343	3.55295	0.04757	102	1572.7	20.2	1514.9	17.46	1539.1	10.61
M20	0.09733	0.00106	0.26271	0.00338	3.52548	0.0471	102	1573.6	20.3	1503.7	17.25	1532.9	10.57

M16	0.0974	0.00105	0.26195	0.00338	3.51734	0.04675	102	1574.9	19.96	1499.8	17.29	1531.1	10.51
M11	0.09758	0.00103	0.27672	0.00356	3.72248	0.04868	100	1578.3	19.53	1574.8	17.97	1576.2	10.47
M6	0.09772	0.00101	0.26126	0.00336	3.5196	0.04551	102	1581	19.16	1496.3	17.17	1531.6	10.22
M12	0.09786	0.00105	0.27902	0.0036	3.76412	0.0497	100	1583.7	19.85	1586.4	18.13	1585.1	10.59
M17	0.09841	0.00106	0.2677	0.00345	3.63182	0.04816	102	1594.2	19.9	1529.1	17.55	1556.5	10.56